Imprints of New Physics in the Angular Distribution of Rare Semileptonic $B \to a_1(\to \rho\pi)l^+l^-$ Decay

By

Nimra Farooq

MS Physics-Fall 2020

Supervisor

Dr. Muhammad Ali Paracha

Department of Physics

School of Natural Sciences (SNS)

National University of Sciences and Technology (NUST)

Islamabad, Pakistan

June 2023

Imprints of New Physics in the Angular Distribution of Rare Semileptonic $B \to a_1(\to \rho\pi)l^+l^-$ Decay

By

Nimra Farooq

MS Physics-Fall 2020

Supervisor

Dr. Muhammad Ali Paracha

A thesis submitted in conformity with the requirements for the degree of *Master of Science* in Physics

Department of Physics

School of Natural Sciences (SNS)

National University of Sciences and Technology (NUST)

Islamabad, Pakistan

July 2022

FORM TH-4

National University of Sciences & Technology

MS THESIS WORK

We hereby recommend that the dissertation prepared under our supervision by: **Nimra Farooq**, Regn No. **00000330860** Titled: **"Imprints OF New Physics in The Angular Distribution of Rare Semileptonic $B \to a_1 (\to p\pi)\, l^+ l^-$ Decay "** accepted in partial fulfillment of the requirements for the award of **MS** degree.

Examination Committee Members

1. Name: DR. AEYSHA KHALIQUE Signature:

2. Name: DR. SAADI ISHAQ Signature:

Supervisor's Name: DR. MUHAMMAD ALI PARACHA Signature:

(FOR) Head of Department 26/6/23 Date

COUNTERSINGED

Date: 26/6/23

Dean/Principal

Dedication

This thesis is dedicated to my family for their endless love, support and encouragement.

Abstract

Rare semileptonic B meson decays induced by $b \to dl^+l^-$ flavor changing neutral current transitions hold immense significance in exploring the quark-flavor sector of the Standard Model and also provide search area to test New Physics. In Standard Model they are not allowed at tree level, but induced by loops and are governed by GIM mechanism. In this work I have studied $B \to a_1(1260)(\to \rho\pi)l^+l^-$ decay which proceed via $b \to d$ transition at quark level. I have focused mainly on physical observables such as branching ratio, forward-backward asymmetry and angular coefficient functions in this decay channel in Standard Model as well as in family non-universal Z' model. Remarkable deviation can be seen from Standard Model values of these physical observables for this decay. It is a clear indication for New Physics appearing due to Z' gauge boson.

Acknowledgments

I would like to thank the almighty GOD for providing me with the opportunity to conduct this research. Thanks to my supervisor Dr. Muhammad Ali Paracha for his extensive guidance and supervision throughout research year. Special thanks to Dr. Faisal Munir for his enormous support and mentorship in conducting this research. Thanks to my dear friend and colleague Marwah Zaki for always being there for me. And finally special thanks to all my friends and family for supporting me in every phase of my life.

Contents

List of Figures

List of Tables

List of Abbreviations

SM	Standard Model
BSM	Beyond Standard Model
NP	New Physics
GIM	Glashow–Iliopoulos–Maiani
EFT	Effective Field Theory
FCNC	Flavor Changing Neutral Current
FCCC	Flavor Changing Charged Current
OPE	Operator Product Expansion
ADM	Anomalous Dimension Matrix
NLO	Next to Leading Order
QCD	Quantum Chromodynamics
BR	Branching Ratio
FBA	Forward Backward Asymmetry
S1	Z' Scenario 1
S2	Z' Scenario 2

Chapter 1

Introduction

The Standard Model of particle physics has proven to be remarkably effective in explaining the fundamental constituents of matter and the fundamental forces that mediate their interactions. However, there are certain limitations that suggests that this theory is not yet complete and needs extension to explain unsolved mysteries of the universe. These limitations include the incorporation of force of gravity within SM. The unification of gravity with other fundamental forces is a significant challenge in modern physics, and it is believed that a more complete theory may be required to address this challenge.

The Standard Model falls short in providing an explanation for the occurrence of dark matter and dark energy. Observations indicate that the observed gravitational effects in the universe cannot be adequately explained by the quantity of visible matter alone. This led to the proposal of presence of dark matter and dark energy, which are believed to comprise a significant portion of the universe's mass-energy.

Neutrinos were originally thought to be massless particles. However, experimental evidence has shown that neutrinos do have a tiny mass, which is not explained by the original Standard Model.

The universe is composed mainly of matter rather than antimatter. This phenomenon is known as matter-antimatter asymmetry. Based on the Standard Model, the Big Bang was expected to generate matter and antimatter in equal proportions, but this is not observed in the universe today.

SM includes the Higgs boson, which is accountable for endowing fundamental particles

with mass. However, the theory also predicts that the Higgs boson's mass should be much larger than the experimentally observed value, leading to what is called the hierarchy problem. This problem refers to the discrepancy between the predicted and observed Higgs boson mass and suggests that there may be additional particles or interactions BSM that help stabilize the Higgs boson mass at a lower value.

These limitations suggest that novel physics surpassing the Standard Model is required to explain these phenomena. The quest for such novel physics represents a highly dynamic field of investigation within the realm of particle physics today.

B-meson decays are a critical area of research in particle physics as they offer promising outcomes for the detection of new physics beyond Standard Model. The deviations of behaviour of B-mesons from SM predicts the presence of unfamiliar particles or interactions that are not yet describe by SM. The processes involving the decay of B-meson to other mesons and a pair of leptons are being studied widely to look for evidences for New Physics. The study of the decay of a B meson to an a_1 meson and a pair of leptons has been found to exhibit discrepancies from the predictions of the SM. The existence of new particles or interactions, such as a new gauge boson or a scalar particle, could provide an explanation for these observed deviations.

To explain the limitations of SM, various extensions are known to exist. One such model that extends the SM is family non-universal Z' model. The family non-universal Z' model is a theoretical extension of the Standard Model that proposes the existence of a new massive gauge boson, known as Z', which would mediate a new force between particles. This model suggests that the Z' boson would couple differently to particles of different generations of fermions, unlike the Standard Model Z boson, which couples equally to all generations of fermions. The study of the family non-universal Z' model is of great interest to particle physicists as it offers promising results for detecting new physics beyond the Standard Model, as deviations from the Standard Model predictions in the production and decay of particles could indicate the presence of the Z' boson or other new particles. Experimental searches for the family non-universal Z' boson are currently in progress at the Large Hadron Collider (LHC) at CERN.

This thesis mainly focuses on the study of decay $B \to a_1(\to \rho\pi)l^+l^-$ in SM and family non-universal Z' model. The goal is to look for deviations from SM values of physical observables for instance branching ratio and FBA, which would indicate for New Physics

and would provide an insight of physics beyond SM. The following presents the specific organization of this thesis:

The 2^{nd} chapter gives the composition of SM i.e. elementary particles and force carriers. It concisely discusses the SM Lagrangian. The basics of Feynman diagrams and the observables studied in particle decays are discussed in brief.

In 3^{rd} chapter, the overview of Flavor physics is given in concise manner. It includes the outline of flavor sector of SM, CKM matrix and its parameterizations. GIM mechanism and the SM flavor puzzle is also reviewed.

The Effective Field Theory is the primary focus of Chapter 4. It focuses mainly on top-down formalism of EFT. Operator Product Expansion and structure of Wilson coefficients are shortly discussed. In last, operator basis for FCNC transitions are given.

Chapter 5 discusses in detail the helicity formalism of $B \to a_1(\to \rho\pi)l^+l^-$ decay. It begins with stating the general Hamiltonian proceeding towards the Hamiltonian for the decay under consideration. It gives matrix elements, form factors, kinematics, lepton helicity amplitude and hadron helicity amplitude for the $B \to a_1$ transition. Then specifically cascade decay $a_1 \to \rho\pi$ is discussed and its kinematics are mentioned. Next angular decay distribution is given and detailed expressions of angular coefficients computed in SM are mentioned. In the end, the family non-universal Z' model is briefly discussed and complete Hamiltonian i.e. SM and Z' model Hamiltonian is specifically mentioned.

In chapter 6, the analysis of physical observables i.e. branching ratio and FBA along with the comparison of angular coefficients in SM and Z' model are discussed in detail. The plots of above mentioned observables are also given and analyzed in detail.

Finally, chapter 7 concludes the results of $B \to a_1(\to \rho\pi)l^+l^-$ decay in SM and family non-universal Z' model.

Chapter 2

The Standard Model of Particle Physics

The exploration of elementary particles and their interactions is the key to understand matter constituents and their properties. Also the major role is played by the forces that allow interactions among these particles. Therefore the Standard Model holds special significance as it provides us with the details of these particles and fundamental forces. This chapter has purpose to give idea about the structure of Standard Model and first section will fulfill the need to get basics of it. Second section is dedicated to the Lagrangian of SM and third one will discuss the Feynman diagrams as they are important to understand particle interactions. Finally in the last section theory of particle decays is discussed as this thesis is based on the study of one such decay. It will help to get an idea about calculations and bit about observables associated with these decays.

2.1 Elements of Standard Model

The understanding of laws on which our universe works is only possible if we know the fundamental building blocks that make up all the existing matter and the forces that exist between the fundamental particles. The SM illustrates the properties of these particles and the forces between them through their exchange. The foundation of the SM lies in the gauge group $G = SU(3)_c \times SU(2)_L \times U(1)_Y$ [1].

2.1.1 The Elementary Particles

Matter comprises electrons with negative charges orbiting around a nucleus composed of positively charged protons and electrically neutral neutrons. Quarks, elementary particles, combine to form the composite particles known as protons and neutrons. Each of proton constitutes two up type quarks and one down type quark and each neutron constitutes two down type and an up type quark. The up-quark, down-quark, electron and electron neutrino are the first generation particles of the Standard Model. The other two generations: second generation and third generation are the exact replicas of the first generation which differ only in masses of particles. The list of twelve fundamental particles: six quarks and six leptons along with their masses and charges is given in Table (2.1) and (2.2).[2]

Quarks			
Generations	**Particle**	**Charge**	**Mass/GeV**
First	down (d)	$-\frac{1}{3}$	0.003
	up (u)	$+\frac{2}{3}$	0.005
Second	strange (s)	$-\frac{1}{3}$	0.1
	charm (c)	$+\frac{2}{3}$	1.3
Third	bottom (b)	$-\frac{1}{3}$	4.5
	top (t)	$+\frac{2}{3}$	174

Table 2.1: The six fundamental quarks

Leptons			
Generations	**Particle**	**Charge**	**Mass/GeV**
First	electron (e^-)	-1	0.0005
	electron neutrino (ν_e)	0	$< 10^9$
Second	muon (μ^-)	-1	0.106
	muon neutrino (ν_μ)	0	$< 10^9$
Third	tau (τ^-)	-1	1.78
	tau neutrino (ν_τ)	0	$< 10^9$

Table 2.2: The six fundamental leptons

Apart from quarks and leptons, there exist gauge bosons, which are responsible for carrying the fundamental forces. In the case of strong interactions, the force is mediated by gluons, which are massless bosons with a spin of 1. For electromagnetic interactions the particle responsible for transmitting the force is the photon which is again spin-1 massless boson and the mediation of weak interactions occurs through W and Z bosons.The forces and their corresponding force-carrying particles along with their relative strengths are given in Table (2.3)

Force	**Strength**	**Boson**	J^P	**Mass/GeV**
Strong	1	Gluon (g)	1^-	0
Electromagnetism	10^{-3}	Photon (γ)	1^-	0
Weak	10^{-8}	W and Z ($W^{\pm}$ and Z)	1^-	80.4 and 91.2
Gravity	10^{-37}	Graviton (hypothetical)	2^+	0

Table 2.3: The four fundamental forces

Another element of the SM is the Higgs Boson. This particle is characterized as a scalar with a spin of 0. It is accountable for the masses of all particles that exist in nature.

2.1.2 The Elementary Forces

The four primary forces consist of the strong force, electromagnetic force, weak force, and gravitational force. Particles engage in interactions with one another via these fundamental forces. Forces experienced by the different particles are given in Table (2.4).

2.1.3 Standard Model Vertices

The interplay among fermions and gauge bosons are described by SM vertices. Properties of the interactions are influenced by the properties of the gauge bosons and nature of the interaction between bosons and fermions.

The three-point vertex involving a gauge boson and an incoming and outgoing fermion represents their interactions as shown in the figures (2.1 - 2.4). A coupling strength denoted by g is associated with each type of interaction.

Particles	Strong force	Electromagnetic force	Weak force
up	Yes	Yes	Yes
down	Yes	Yes	Yes
charm	Yes	Yes	Yes
strange	Yes	Yes	Yes
top	Yes	Yes	Yes
bottom	Yes	Yes	Yes
electron	No	Yes	Yes
muon	No	Yes	Yes
tau	No	Yes	Yes
electron neutrino	No	No	Yes
muon neutrino	No	No	Yes
tau neutrino	No	No	Yes

Table 2.4: The forces encountered by various particles

Strong Force

The strong force acts between all quarks since only quarks contain the color charge of QCD. Quark flavor does not change in strong interaction as it conserves all flavors. The strong coupling constant is a dimensionless quantity and the nature of the interaction can vary depending on the energy scale at which it occurs. At low energies, the strong coupling constant exhibits a significant magnitude that means quarks interact very strongly with each other. At higher energies, the strong coupling constant becomes smaller, meaning that quarks interact less strongly with each other. The inherent magnitude of the QCD interaction is approximately given by $g_S \sim 1$, which is much larger than the values of the other fundamental forces. This is the reason why the strong force is acknowledged as the most powerful among the fundamental forces at the energy scales relevant for nuclear physics.

Electromagnetism

The electromagnetic force applies to every charged particle, exerting an influence between them. There is no change in flavor in electromagnetic interaction. The fine structure constant is a parameter that quantifies the magnitude of the electromagnetic

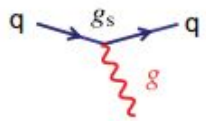

Figure 2.1: Strong Force

force, which is a dimensionless quantity. The intrinsic strength of this interaction is $e \sim \frac{1}{137}$.

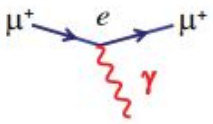

Figure 2.2: Electromagnetism

Weak Charged Current

The weak charged-current interaction connects pairs of fundamental fermions that have a disparity of one electric charge unit. It is the only interaction which involves change of flavor. The intrinsic strength of weak charged-current interaction is $g_W \sim \frac{1}{30}$.

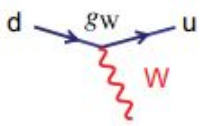

Figure 2.3: Weak Charged Current

Weak Neutral Current

The weak neutral-current interaction is between all fundamental fermions. There is no change of flavor in this interaction as well. The intrinsic strength of weak neutral-current interaction is $g_Z \sim \frac{1}{30}$.

2.2 Standard Model Lagrangian

The SM Lagrangian density is written as [1]

$$\mathcal{L}_{SM} = \mathcal{L}_{gauge} + \mathcal{L}_{fermion} + \mathcal{L}_{HIggs} + \mathcal{L}_{Yukawa} \tag{2.2.1}$$

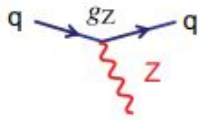

Figure 2.4: Weak Neutral Current

$\mathcal{L}_{gauge}$ term refers to the kinetic energies pertaining to the gauge fields and are written as

$$\mathcal{L}_{gauge} = -\frac{1}{4}G^i_{\mu\nu}G^{\mu\nu i} - \frac{1}{4}W^i_{\mu\nu}W^{\mu\nu i} - \frac{1}{4}B_{\mu\nu}B^{\mu\nu} \tag{2.2.2}$$

where

$$G^i_{\mu\nu} = \partial_\mu G^i_\nu - \partial_\nu G^i_\mu - g_s f_{ijk} G^j_\mu G^k_\nu \qquad ; i,j,k = 1...8,$$
$$W^i_{\mu\nu} = \partial_\mu W^i_\nu - \partial_\nu W^i_\mu - g\epsilon_{ijk} W^j_\mu W^k_\nu \qquad ; i,j,k = 1...3,$$

and

$$B_{\mu\nu} = \partial_\mu B_\nu - \partial_\nu B_\mu$$

represents the field strength tensors for SU(3), SU(2) and U(1) respectively.

$\mathcal{L}_{fermion}$ refers to the fermionic part of the SM. Fermions include three families of quarks and leptons each consisting L-chiral SU(2) doublets and R-singlets represented as

$$L - doublets: \qquad q^0_{mL} = \begin{pmatrix} u^0_m \\ d^0_m \end{pmatrix}_L, \qquad l^0_{mL} = \begin{pmatrix} \nu^0_m \\ e^{-0}_m \end{pmatrix}_L$$

and

$$R - singlets: \qquad u^0_{mR}, \quad d^0_{mR}, \quad e^{-0}_{mR}, \quad \nu^0_{mR}.$$

where superscript ^{0} refers to having definite gauge transformation properties and $m = 1...3$ labels the family number.

$\mathcal{L}_{fermion}$ consists of gauge-covariant kinetic energy terms, it can be written as

$$\mathcal{L}_{fermion} = \sum_{m=1}^{3} (\overline{q}^0_{mL}\iota\not{D}q^0_{mL} + \overline{l}^0_{mL}\iota\not{D}l^0_{mL} + \overline{u}^0_{mR}\iota\not{D}u^0_{mR} + \overline{d}^0_{mR}\iota\not{D}d^0_{mR} + \overline{e}^0_{mR}\iota\not{D}e^0_{mR} + \overline{\nu}^0_{mR}\iota\not{D}\nu^0_{mR}) \tag{2.2.3}$$

The Higgs part $\mathcal{L}_{Higgs}$ of standard model Lagrangian can be expressed as

$$\mathcal{L}_{Higgs} = (D^\mu\phi)^\dagger D_\mu\phi - V(\phi) \tag{2.2.4}$$

where $\phi = \begin{pmatrix} \phi^\dagger \\ \phi^0 \end{pmatrix}$ is a complex Higgs scalar and $D_\mu\phi$ is the gauge covariant derivative, represented as

$$D_\mu\phi = (\partial_\mu + \frac{\iota g}{2}\vec{\tau}.\vec{W}_\mu + \frac{\iota g'}{2}B_\mu)\phi$$

$V(\phi)$ is the Higgs potential, it's mathematical form is

$$V(\phi) = \mu^2\phi^\dagger\phi + \lambda(\phi^\dagger\phi)^2$$

$\mathcal{L}_{Yukawa}$ refers to the Yukawa couplings among Higgs doublet and the fermions. It can be written as

$$\mathcal{L}_{Yukawa} = -\sum_{m,n=1}^{F} [\Gamma^u_{mn}\overline{q}^0_{mL}\tilde{\phi}u^0_{nR} + \Gamma^d_{mn}\overline{q}^0_{mL}\phi d^0_{nR} + \Gamma^e_{mn}\bar{l}^0_{mn}\phi e^0_{nR} + \Gamma^\nu_{mn}\bar{l}^0_{mL}\tilde{\phi}\nu^0_{nR}] + h.c. \tag{2.2.5}$$

where $\phi = \begin{pmatrix} \phi^\dagger \\ \phi^0 \end{pmatrix}$ and $\tilde{\phi} = \begin{pmatrix} \phi^{0\dagger} \\ -\phi^- \end{pmatrix}$ are the Higgs doublet and its conjugate. F is the fermion family number. $\Gamma^u, \Gamma^d, \Gamma^e, \Gamma^\nu$ are the $F \times F$ matrices which determine the masses and mixings of fermions.

2.3 Feynman Diagrams

Feynman diagrams let us compute scattering amplitudes of the interactions between elementary particles. They are a pictorial representation of particle interactions that are used to visualize and calculate the probability of a particular outcome in a physical process. They contains the following:

External Lines

External lines denote the particles entering and exiting in a scattering or decay process. Spin $\frac{1}{2}$ particles and anti-particles are represented by straight lines with arrows on them. Arrows indicate the direction of particle flow along the lines. Arrows on anti-particles are in negative time direction. Spin 1 particles are represented by wavy lines.

Vertices

Vertices are locations where lines representing particles converge, facilitating their interactions with one another. They represent the point at which a particle emits or absorbs another particle. A vertex will have three or four lines attached. At each vertex energy, momentum, angular momentum, charge, lepton number, baryon number, strangeness and parity (except in weak interactions) are conserved.

Internal Lines

Internal lines represents propagators (virtual particles). Spin $\frac{1}{2}$ particles are indicated

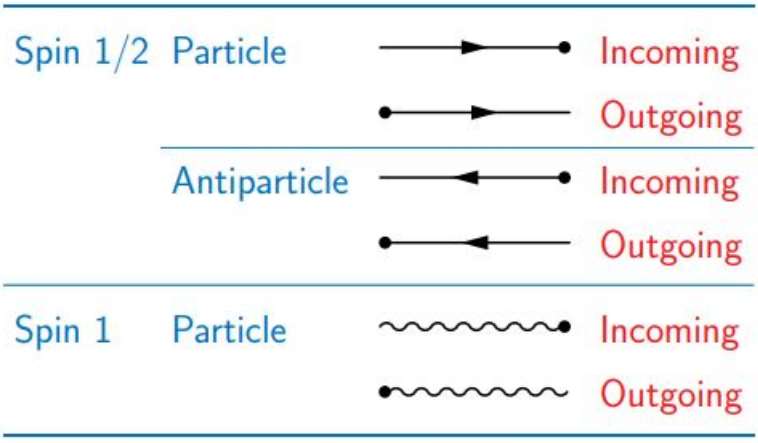

Figure 2.5: External Lines in Feynman Diagrams

by straight lines and spin 1 particles are indicated by wavy or wiggly lines between two vertices.

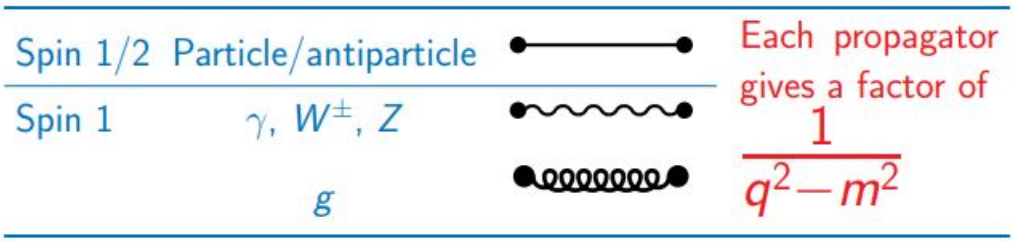

Figure 2.6: Internal Lines in Feynman Diagrams

Loops

Loops represent virtual particles that are created and annihilated immediately, without ever being directly observed.

Momentum

Momentum of a particle is indicated by the lines and arrows in the diagram. The direction of the arrow on a line suggests the direction of particle's momentum, while the length of the arrow is proportional to the magnitude of momentum.

2.3.1 Feynman Rules for Quantum Electrodynamics

External Lines

Incoming $u(p)$ and outgoing $\overline{u}(p)$ spin $\frac{1}{2}$ particles are represented as:

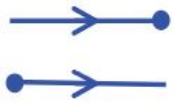

Figure 2.7: Incoming and outgoing spin $\frac{1}{2}$ particle

Incoming $v(p)$ and outgoing $\overline{v}(p)$ spin $\frac{1}{2}$ anti-particles are represented as:

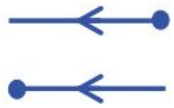

Figure 2.8: Incoming and outgoing spin $\frac{1}{2}$ anti-particle

Incoming $\varepsilon^{\mu}(p)$ and outgoing $\varepsilon^{\mu}(p)^{*}$ photon is represented as:

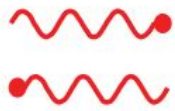

Figure 2.9: Incoming and outgoing photon

Internal Lines

Photon $-\frac{\iota g_{\mu\nu}}{q^2}$ is represented as:

Figure 2.10: Photon Propagator

Spin $\frac{1}{2}$ fermion $\frac{\iota(\gamma^{\mu}q_{\mu}+m)}{q^2-m^2}$ is represented as:

Figure 2.11: Fermion Propagator

Vertex

Spin $\frac{1}{2}$ fermion with charge -|e| $\iota e\gamma^{\mu}$ vertex is represented as:

Figure 2.12: Fermion Vertex

2.3.2 Feynman Rules for Quantum Chromodynamics

External Lines

Incoming $u(p)$ and outgoing $\overline{u}(p)$ spin $\frac{1}{2}$ quarks are represented as:

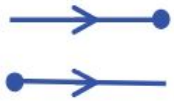

Figure 2.13: Incoming and outgoing spin $\frac{1}{2}$ quark

Incoming $v(p)$ and outgoing $\overline{v}(p)$ spin $\frac{1}{2}$ anti-quarks are represented as:

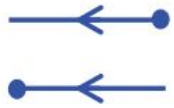

Figure 2.14: Incoming and outgoing spin $\frac{1}{2}$ anti-quark

Incoming $\varepsilon^{\mu}(p)$ and outgoing $\varepsilon^{\mu}(p)^{*}$ gluon is represented as:

Figure 2.15: Incoming and outgoing gluon

Internal Lines

Gluon $-\frac{\iota g_{\mu\nu}}{q^2}\delta^{ab}$, where $a, b = 1, 2, ..., 8$ are gluon color indices, is represented as:

Figure 2.16: Gluon Propagator

Vertex

Spin $\frac{1}{2}$ quark $-\iota g_s \frac{1}{2}\lambda^a_{ji}\gamma^\mu$, where $i, j = 1, 2, 3$ are quark colors and a=1,2,...,8 are the Gell-Mann SU(3) matrices, vertex is represented as:

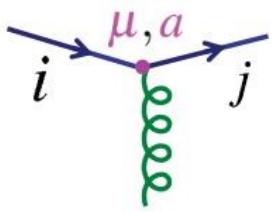

Figure 2.17: Quark Vertex

2.4 Study of Particle Decays

2.4.1 Lifetime and Decay Rate

Lifetime is one of the most significant characteristic of a particle and it depends on its available decay modes. It is a statistical distribution and is specified for a large sample. The lifetime of an individual particle is the time after which the ensemble is expected to reduce to $\frac{1}{e}$ of its original size [3]. It is mathematically represented as

$$\tau = \frac{1}{\Gamma} \tag{2.4.1}$$

where Γ is the decay rate which is the probability of a particular particle decaying per unit of time.

In the case of an ensemble consisting of a large number of identical particles ($N \to \infty$), the alteration in the particle count over a time interval dt can be expressed as follows.

$$dN = -\Gamma N dt \tag{2.4.2}$$

After time t, the number of surviving particles is

$$N(t) = N(0)e^{-\Gamma t} \tag{2.4.3}$$

A decay rate is associated with each decay mode. All possible final states of a particle are its decay modes. Each decay mode has its own matrix element. The total decay rate is obtained by combining the rates of individual decay modes. It is given by

$$\Gamma_{total} = \sum_{i=1}^{n} \Gamma_i \tag{2.4.4}$$

The particle's lifetime in terms of total decay rate is given by

$$\tau = \frac{1}{\Gamma_{total}}. \tag{2.4.5}$$

The branching fraction is a measure of the probability that a particular decay mode will occur for a given particle. It is described as the ratio of the decay rate of a particular decay mode and the overall decay rate of the particle.

$$\mathcal{B}_i = \frac{\Gamma_i}{\Gamma_{total}}. \tag{2.4.6}$$

2.4.2 Scattering Cross Section

The scattering cross section indicates the probability that two particles will scatter off each other when they interact. Consider a scenario where a beam of particles a, with velocity β_a, collide with a stationary target of particles b. This collision follows the reaction formula $a + b \rightarrow c + d$. The cross section for a collision between two particles is defined as follows: [4]

$$d\sigma = \frac{d\omega_{fi}}{j} \tag{2.4.7}$$

where $d\omega_{fi}$ represents the probability of transitioning from an initial state i to a final state f and j represents incident flux. The cross section for such collision is given by

$$d\sigma = \frac{1}{2E_a\beta_a 2M_b}|\mathcal{M}|^2 d\Phi. \tag{2.4.8}$$

For two body decay, $d\Phi$ is calculated as

$$d\Phi = \int \frac{(2\pi)^4}{4(2\pi)^6}\delta^4(p_a + p_b - p_c - p_d)\frac{d^3p_c}{E_c}\frac{d^3p_d}{E_d} \tag{2.4.9}$$

where p_a, p_b, p_c and p_d are the 3-momenta of particles a,b,c and d respectively.

Putting the above expression in equation (2.4.8) gives

$$d\sigma = \frac{1}{2E_a\beta_a 2M_b}|\mathcal{M}|^2 \int \frac{(2\pi)^4}{4(2\pi)^6}\delta^4(p_a + p_b - p_c - p_d)\frac{d^3p_c}{E_c}\frac{d^3p_d}{E_d}. \tag{2.4.10}$$

The scattering cross section gives information about the nature of the interaction between particles and can be used to test theoretical models of particle interactions. It is essential for understanding the behavior of particles and for interpreting experimental results.

Chapter 3

Flavor Physics

The term "flavor" in particle physics was first used by Murray Gell-Mann and his student, Harald Fritzsch, in 1971 [5]. In Standard Model, flavor physics addresses the interactions and properties of matter constituents which are excitations in fermionic (spin = 1/2) fields. It is the physics of three generations of quarks and leptons that exists in nature. These three generations have all equal gauge couplings i.e, they all behave equally under gauge interactions. However they are different in masses and also different in Yukawa interactions. Flavor physics, in the context of the Standard Model, pertains to Yukawa interactions that discriminate between various flavors. [6]. Due to these differences there are flavor violating effects and due to Yukawa interactions there are flavor changing interactions. From Yukawa couplings we get flavor mixing, therefore, we get flavor changing couplings and that is why heavier quarks and leptons decay into lighter flavors.

Flavor physics to great extent deals with the ways these decays occur, how likely or how rare they are, making predictions within Standard Model and looking into what we measure in actuality agree upon with these predictions.

Flavor Parameters: The term "flavor parameters" indicates parameters that are associated with different flavors of elementary particles. In the SM of particle physics, flavor parameters include harged fermion massses and mixing parameters that depict the interactions between quark-antiquark pairs and the charged weak-force carriers (W±).

Flavor Universal: In the realm of particle physics, the term "flavor universal" characterizes interactions in which the couplings or flavor parameters exhibit correlation with the unit matrix within the flavor space. This means that the strength of the interaction does not depend on the specific flavor of the interacting particles. Another term for

"flavor universal" is "flavor blind." Both terms refer to interactions in which the strength does not depend on the specific flavor of the particles involved.

Flavor Diagonal: The term "flavor diagonal" indicates interactions in particle physics where the couplings or flavor parameters are diagonal in the flavor space. This means that the interaction only occurs between particles of the same flavor, and the strength of the interaction may vary depending on the specific flavor of the interacting particles.

Flavor Changing: The term "flavor changing" indicates processes where difference between the initial and final quantities of particles belonging to a specific flavor (taking into account quantity of corresponding antiparticles) is not equal. In "flavor-changing charged current" processes, both up-type and down-type flavors, and/or both charged lepton and neutrino flavors, are present. These processes are transmitted by the W bosons and takes place at the tree level within the Standard Model. In 'flavor-changing neutral current' (FCNC) processes, either up-type or down-type flavors but not both, and/or either charged lepton or neutrino flavors but not both, participates. These processes do not occur at the tree level within the Standard Model and are often highly suppressed.

Flavor Violation: Flavor violation refers to a phenomenon in particle physics where the flavor of a particle changes in a way that is not permitted by the SM of particle physics.

This chapter includes main ideas in study of flavor physics. The first section is about the flavor sector of SM. Next section deals with CKM matrix and its parameterizations. Last two sections are about GIM mechanism and the SM flavor puzzle.

3.1 The Flavor Sector of Standard Model

The two main parts of Standard Model are the SM gauge and Higgs sector. The gauge sector is fully specified by local symmetry as [7]

$$\mathcal{G}^{SM}_{local} = SU(3)_C \times SU(2)_L \times U(1)_Y \tag{3.1.1}$$

and by fermion content as

$$\mathcal{L}^{SM}_{gauge} = \sum_{i=1,\dots,3} \sum_{\psi=Q^i_L,\dots,E^i_R} \overline{\psi} \not{D} \psi - \frac{1}{4} \sum_{a=1,\dots,8} G^a_{\mu\nu} G^a_{\mu\nu} - \frac{1}{4} \sum_{a=1,\dots,3} W^a_{\mu\nu} W^a_{\mu\nu} - \frac{1}{4} B_{\mu\nu} B_{\mu\nu} \tag{3.1.2}$$

where $\not{D} \equiv D_\mu \gamma^\mu$ with D_μ being a covariant derivative.

The fermionic sector of SM contains five distinct fields characterized by different quantum numbers under the gauge group,

$$Q_L^i(3,2)_{+\frac{1}{6}}, \quad U_R^i(3,1)_{+\frac{2}{3}}, \quad D_R^i(3,1)_{-\frac{1}{3}}, \quad L_L^i(1,2)_{-\frac{1}{2}}, \quad E_R^i(1,1)_{-1},$$

each with three generations (i=1,2,3). This leads to the global flavor symmetry of $\mathcal{L}_{gauge}^{SM}$. These global and local symmetries are broken by Higgs field . The local symmetry undergoes spontaneous symmetry breaking through the vacuum expectation value of the Higgs field, $\langle\phi\rangle \approx 174$ GeV whereas the global flavor symmetry undergoes breaking due to Yukawa interaction between the Higgs field and fermionic fields, as expressed by the following equation

$$-\mathcal{L}_{Yukawa}^{SM} = Y_d^{ij}\overline{Q}_L^i \phi D_R^j + Y_u^{ij}\overline{Q}_L^i \tilde{\phi} U_R^j + Y_e^{ij}\overline{L}_L^i \phi E_R^j + h.c. \tag{3.1.3}$$

where $\tilde{\phi} = \iota\tau_2\phi^\dagger$.

3.2 The Cabibbo-Kobayashi-Maskawa (CKM) Quark-Mixing Matrix

The masses and mixings of quarks emerge from Yukawa interactions with the Higgs condensate. To study these Yukawa interactions, the two necessary basis rotations are mass basis and interaction basis. In mass basis the masses are diagonal and in interaction basis the weak ($W^\pm$) interactions are diagonal. The CKM mixing matrix describes the complex rotation between the mass eigenstates and weak interaction eigenstates. It is a 3×3 unitary matrix [8],[9] parameterized by three mixing angles and quark mixing phase. It controls the conversion of one quark to another and in this process W boson is produced. The elements of CKM matrix can be expressed as

$$V_{CKM} = \begin{pmatrix} V_{ud} & V_{us} & V_{ub} \\ V_{cd} & V_{cs} & V_{cb} \\ V_{td} & V_{ts} & V_{tb} \end{pmatrix}$$

3.2.1 Standard Parametrization

The standard parameterization of V_{CKM} is given by [10]

$$V_{CKM} = \begin{pmatrix} c_{12}c_{13} & s_{12}c_{13} & s_{13}e^{-\iota\delta} \\ -s_{12}c_{23} - c_{12}s_{23}s_{13}e^{\iota\delta} & c_{12}c_{23} - s_{12}s_{23}s_{13}e^{\iota\delta} & s_{23}c_{13} \\ s_{12}s_{23} - c_{12}c_{23}s_{13}e^{\iota\delta} & -c_{12}s_{23} - s_{12}c_{23}s_{13}e^{\iota\delta} & c_{23}c_{13} \end{pmatrix}$$

where $c_{ij} \equiv \cos\theta_{ij}$ and $s_{ij} \equiv \sin\theta_{ij}$. The $\sin\theta_{ij}$ represents three real mixing parameters whereas δ represents Kobayashi-Maskawa phase.

3.2.2 Wolfenstein Parametrization

Wolfenstein parameterization of CKM matrix contains four mixing parameters i.e, λ, A, ρ and η where η is CP Violating phase and λ is expansion parameter with value [11]

$$\lambda = |V_{us}| \approx 0.22$$

Wolfenstein parameterization to order $\mathcal{O}(\lambda^4)$ is as follows

$$V_{CKM} = \begin{pmatrix} 1 - \frac{\lambda^2}{2} & \lambda & A\lambda^3(\rho - \iota\eta) \\ -\lambda & 1 - \frac{\lambda^2}{2} & A\lambda^2 \\ A\lambda^3(1 - \rho - \iota\eta) & -A\lambda^2 & 1 \end{pmatrix}$$

The matrix elements of V_{CKM} are related to eachother through its unitarity property as

$$\sum_i V_{id}V_{is}^* = 0 \tag{3.2.1}$$

For the total of three complex quantities to disappear such as

$$V_{ud}V_{ub}^* + V_{cd}V_{cb}^* + V_{td}V_{tb}^* = 0 \tag{3.2.2}$$

requires six relations just like the one written in equation (3.3.1). They are geometrically represented in the form of triangle known as 'The unitarity triangles' in complex plane. All unitarity triangles of CKM matrix have similar areas that is equivalent to half of Jarlskog invariant $\mathcal{J}$ [12] defined as

$$\Im[V_{ij}V_{kl}V_{il}^*V_{kj}^*] = \mathcal{J}\sum_{m,n}\epsilon_{ikm}\epsilon_{jln} \tag{3.2.3}$$

where $i, j, k, l = 1, 2, 3$.

The lengths, vertices and angles of unitarity triangle in the wolfenstein parameterization is shown in figure (3.1)

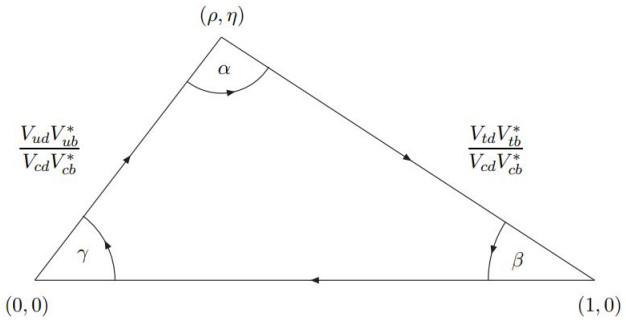

Figure 3.1: The unitarity triangle

where lengths of two complex sides are denoted as

$$\left|\frac{V_{ud}V_{ub}}{V_{cd}V_{cb}}\right| = \sqrt{\rho^2+\eta^2},$$
$$\left|\frac{V_{td}V_{tb}}{V_{cd}V_{cb}}\right| = \sqrt{(1-\rho)^2+\eta^2}.$$

and three angles are denoted as

$$\alpha \equiv \arg\left[-\frac{V_{td}V_{tb}^*}{V_{ud}V_{ub}^*}\right],$$
$$\beta \equiv \arg\left[-\frac{V_{cd}V_{cb}^*}{V_{td}V_{tb}^*}\right],$$
$$\gamma \equiv \arg\left[-\frac{V_{ud}V_{ub}^*}{V_{cd}V_{cb}^*}\right].$$

3.3 GIM Mechanism

The GIM Mechanism was introduced by Sheldon L. Glashow, John Iliopoulos and Luciano Maiani in 1970, which aims to clarify why $\Delta S = 1, 2$ neutral current processes are inhibited[13]. In SM, weak interactions involve exchange of W and Z bosons, which couple to particles with different flavors. However, in the absence of GIM mechanism, this would lead to the existence of FCNCs, where particles would change flavor without any apparent reason. GIM mechanism explains the observed suppression of FCNCs in weak interactions. The mechanism relies on the existence of a family of four quarks, where each quark has a corresponding weak eigenstate. The mixing of weak eigenstates of quarks gives rise to observed mass eigenstates, which are states that are actually observed experimentally.

3.4 The Standard Model Flavor Puzzle

In SM, there are 13 flavor parameters, including six quark Yukawa couplings, four CKM parameters, and three charged lepton Yukawa couplings. While top-Yukawa and KM phase are of order 1, the remaining parameters display characteristics of small size and a clear hierarchical structure., spanning six orders of magnitude. The orders of magnitudes of the thirteen dimensionless flavor parameters are given below. [6, 14]

$$y_u \sim 0.00001, \quad y_c \sim 0.01, \quad y_t \sim 1,$$

$$y_d \sim 0.0001, \quad y_s \sim 0.001, \quad y_b \sim 0.01,$$

$$y_e \sim 0.000001, \quad y_\mu \sim 0.001, \quad y_\tau \sim 0.01,$$

$$|V_{us}| \sim 0.2, \quad |V_{cb}| \sim 0.04, \quad |V_{ub}| \sim 0.004, \quad \delta_{KM} \sim 1$$

The reason for this smallness and hierarchy is still unclear and is known as the Standard Model flavor puzzle. Finding a solution to this puzzle may provide insights into physics beyond the Standard Model.

Chapter 4

Effective Field Theory

The physical phenomena in our universe are observed at all scales i.e. we observe structures that are as large as the universe itself or as small as quarks and leptons that make up atoms and all of matter. When we study these phenomena we might need to choose the scale that is best suited depending on what we are observing exactly. In this regard Effective Field Theory is a tool that is used to pick out the suitable scale to study our observation as it deals with multi scale problems and allow us to analyze physical systems at different scales. EFT of any physical system gives us dynamics of this system at low energies without requiring complete details at much higher energies.

EFT of any physical system is built by applying one of the two following standard procedures:

i. Top-down, and

ii. Bottom-up.

In top-down approach we know the behaviour of physical system at higher energies and by integrating out heavier particles or by choosing a cutoff below that higher energy we match onto a physical system at lower energies via path integral formalism. This approach gives us new operators and couplings at these lower energies.

In bottom-up approach , since we have no idea about the physical system at higher energies, therefore the Lagrangian is assembled by considering all possible set of interactions that are consistent with the symmetries and using fields for the applicable degrees of freedom.

In this chapter I'll discuss in bit detail about top-down approach to construct an EFT

and will get our desired action. Then this non-local action is expanded in terms of local operators by applying Operator Product Expansion. This will result in Lagrangian of our interest. This Lagrangian is an infinite sum over local operators multiplied by coupling constants known as Wilson Coefficients [15].

4.1 Top-Down Formalism

Contemplate a quantum field theory as a system with known behaviour at higher energies or simply with large and definite underlying scale $\mathcal{E}$. Let we need to deal with such a system but at some lower scale that is smaller than $\mathcal{E}$. This can be done by choosing a cutoff scale $\Lambda < \mathcal{E}$ and splitting the fields ϕ of the theory among low-frequency and high-frequency modes as

$$\phi = \phi_L + \phi_H \tag{4.1.1}$$

where ϕ_L carries low-frequency $\omega < \Lambda$ modes , whereas ϕ_H carries high-frequency $\omega > \Lambda$ modes. This way physical observables for example decay rates and cross sections etc can be calculated by using vacuum correlation function of the low-frequency mode fields ϕ_L as after dividing the fields the low energy details are inscribed in ϕ_L part.

The vacuum correlation functions are the vacuum expectation values of time-ordered products of field operators. These correlation functions can be used to calculate the physical observables. The correlators can be acquired by using

$$\langle 0|T\{\phi_L(x_1)\phi_L(x_2)...\phi_L(x_n)\}|0\rangle = \frac{1}{Z[0]}\Big(-\iota\frac{\delta}{\delta J_L(x_1)}\Big)\Big(-\iota\frac{\delta}{\delta J_L(x_2)}\Big)... \\ ...\Big(-\iota\frac{\delta}{\delta J_L(x_n)}\Big)Z[J_L]\Big|_{J_L=0} \tag{4.1.2}$$

where

$$Z[J_L] = \int \mathcal{D}\phi_L\mathcal{D}\phi_H e^{\iota S(\phi_L,\phi_H)+\iota\int d^D x J_L(x)\phi_L(x)} \tag{4.1.3}$$

denotes generating functional of the theory,

$$S(\phi_L,\phi_H) = \int d^D x\mathcal{L}(x) \tag{4.1.4}$$

denotes the action, D represents space-time dimension, and J_L are sources for low-frequency mode fields.

The high-frequency modes pertaining to the fields can be integrated out by performing path integral formalism over these fields. This alters the generating functional as

$$Z[J_L] = \int \mathcal{D}\phi_L e^{\iota S_\Lambda(\phi_L) + \iota \int d^D x J_L(x)\phi_L(x)} \tag{4.1.5}$$

where

$$e^{\iota S_\Lambda(\phi_L)} = \int \mathcal{D}\phi_H e^{\iota S(\phi_L, \phi_H)} \tag{4.1.6}$$

is known as the Wilsonian effective action. This process has freed the functional integral from high-frequency mode fields and due to this removal of high frequency fluctuations from the integral has caused the effective action S_Λ to become non-local on $\frac{1}{\Lambda}$ scales.

4.2 Operator Product Expansion

The non-local action functional S_Λ derived in the last section can be expanded in terms of local operators in process called Operator Product Expansion (OPE). This results in action as

$$S_\Lambda(\phi_L) = \int d^D x \mathcal{L}_\Lambda^{eff}(x) \tag{4.2.1}$$

where

$$\mathcal{L}_\Lambda^{eff}(x) = \sum_{D,i} \frac{\mathcal{C}_i^{(D)}}{\mathcal{E}^{D-d}} \mathcal{O}^{(D)}(\phi_L(x)) \tag{4.2.2}$$

is the local effective Lagrangian.

The Lagrangian in equation (4.3.2) contains an infinite series of operators with mass dimension D. Coefficients of these operators $\mathcal{C}_i^{(D)} \mathcal{E}^{d-D}$ are known as Wilson Coeffients.

4.3 The General Structure of Wilson Coefficients

The general expression for Wilson Coefficients C_i can be written as [16]

$$\vec{C}(\mu) = \hat{U}(\mu, M_W)\vec{C}(M_W) \tag{4.3.1}$$

where $\vec{C}(\mu)$ represents a column vector, and μ is the scale which segregates the physics contained in short distance (scale $> \mu$) from long distance (scale $< \mu$). $\vec{C}(M_W)$ are initial conditions that relies on higher energy scales and $\hat{U}(\mu, M_W)$ represents evolution matrix.

Renormalization-group equation for $\vec{C}$ is written as [17]

$$\frac{d}{d(ln\mu)}\vec{C}(\mu) = \gamma^T(g_s)\vec{C}(\mu) \tag{4.3.2}$$

where $\gamma^T(g_s)$ represents anomalous dimension matrix of operator $\mathcal{O}$ and it relies on scale μ running through QCD coupling $\alpha_s(\mu)$. The same renormalization-group equation as for $\vec{C}$ can also be written for $\hat{U}(\mu, M_W)$ as

$$\frac{d}{d(ln\mu)}\hat{U}(\mu, M_W) = \gamma^T(g_s)\hat{U}(\mu, M_W) \tag{4.3.3}$$

General solution for above equation can be written as

$$\hat{U}(\mu, M_W) = T_g e^{\left[\int_{g(M_W)}^{g(\mu)} dg_s \frac{\gamma^T(g_s)}{\beta(g_s)}\right]} \tag{4.3.4}$$

where T_g is the g-ordering operator and $\beta(g_s)$ is renormalization group function which controls evolution of coupling constant $\alpha_s(\mu)$. $\hat{U}(\mu, M_W)$ sums large logarithms $ln(\frac{M_W}{\mu})$ which emerge for $\mu << M_W$.

The expansion of ADM $\gamma(\alpha_s)$ in powers of (α_s) and $\beta(g_s)$ in powers of g_s can be expressed as

$$\gamma(\alpha_s) = \gamma^{(0)}\frac{\alpha_s}{4\pi} + \gamma^{(1)}(\frac{\alpha_s}{4\pi})^2 + ..., \tag{4.3.5}$$

and

$$\beta(g_s) = -\beta_0\frac{g_s^3}{16\pi^2} - \beta_1\frac{g_s^5}{(16\pi^2)^2} - ... \tag{4.3.6}$$

respectively. Putting equations (4.3.5) and (4.3.6) into equation (4.3.4) results in

$$\hat{U}(\mu, M_W) = \left[1 + \frac{\alpha_s(\mu)}{4\pi}\right]\left[\frac{\alpha_s(M_W)}{\alpha_s(\mu)}\right]^P\left[1 - \frac{\alpha_s(M_W)}{4\pi}J\right] \tag{4.3.7}$$

where $J = \frac{P}{\beta_0}\beta_1 - \frac{\gamma^{(1)}}{2\beta_0}$ and $P = \frac{\gamma^{(0)}}{2\beta_0}$.

At NLO the expression for $C(M_W)$ can be written as [18]

$$C(M_W) = 1 + \frac{\alpha_s(M_W)}{4\pi}B \tag{4.3.8}$$

Putting equations (4.4.7) and (4.4.8) into equation (4.4.1), we get an equation for $C(\mu)$ in NLO approximation

$$C(\mu) = \left[1 + \frac{\alpha_s(\mu)}{4\pi}\right]\left[\frac{\alpha_s(M_W)}{\alpha_s(\mu)}\right]^P\left[1 + \frac{\alpha_s(M_W)}{4\pi}(B - J)\right]. \tag{4.3.9}$$

4.4 Operator Basis for FCNC Transitions

The Standard Model operator basis for FCNC transitions include the following operators:

Current-Current Operators

$$\mathcal{O}_1 = (\overline{s}_i u_j)_{V-A}(\overline{u}_j d_i)_{V-A},$$
$$\mathcal{O}_2 = (\overline{s}u)_{V-A}(\overline{u}d)_{V-A}.$$

The diagrams for Current-Current Operators is given in Figure (4.1).

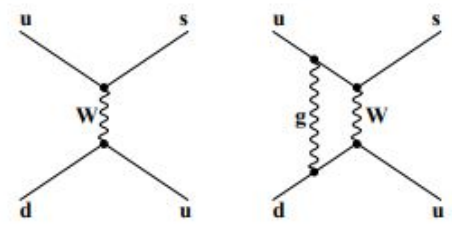

Figure 4.1: Current-Current Operators

QCD Penguin Operators

$$\mathcal{O}_3 = (\overline{s}d)_{V-A}\sum_q(\overline{q}q)_{V-A},$$
$$\mathcal{O}_4 = (\overline{s}_i d_j)_{V-A}\sum_q(\overline{q}_j q_i)_{V-A},$$
$$\mathcal{O}_5 = (\overline{s}d)_{V-A}\sum_q(\overline{q}q)_{V+A},$$
$$\mathcal{O}_6 = (\overline{s}_i d_j)_{V-A}\sum_q(\overline{q}_j q_i)_{V+A}.$$

The diagram for QCD Penguin Operators is given in Figure (4.2).

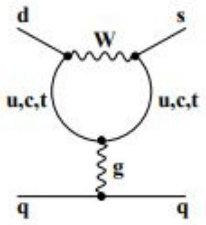

Figure 4.2: QCD Penguin Operators

Electroweak Penguin Operators

$$\mathcal{O}_7 = \frac{3}{2}(\bar{s}d)_{V-A}\sum_q e_q(\bar{q}q)_{V+A},$$
$$\mathcal{O}_8 = \frac{3}{2}(\bar{s}_i d_j)_{V-A}\sum_q e_q(\bar{q}_j q_i)_{V+A},$$
$$\mathcal{O}_9 = \frac{3}{2}(\bar{s}d)_{V-A}\sum_q e_q(\bar{q}q)_{V-A},$$
$$\mathcal{O}_{10} = \frac{3}{2}(\bar{s}_i d_j)_{V-A}\sum_q e_q(\bar{q}_j q_i)_{V-A}.$$

The diagrams for Electroweak Penguin Operators is given in Figure (4.3).

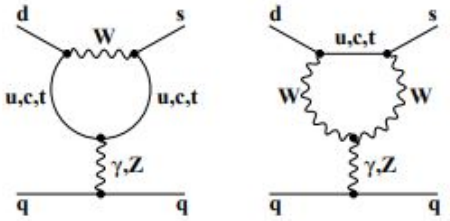

Figure 4.3: Electroweak Penguin Operators

Magnetic Penguin Operators

$$\mathcal{O}_{7\gamma} = \frac{e}{8\pi^2} m_b \bar{s}_i \sigma^{\mu\nu}(1+\gamma_5) b_i \mathcal{F}_{\mu\nu},$$
$$\mathcal{O}_{8G} = \frac{g}{8\pi^2} m_b \bar{s}_i \sigma^{\mu\nu}(1+\gamma_5) \mathcal{T}^a_{ij} b_j \mathcal{G}^a_{\mu\nu}.$$

where $\mathcal{F}_{\mu\nu}$ is the electromagnetic field strength tensor, $\mathcal{G}^a_{\mu\nu}$ represents gluon field strength tensor and $\mathcal{T}^a_{ij}$ are generators of the SU(3) color group. Operator $\mathcal{O}_{7\gamma}$ represents photo-magnetic penguin operator and $\mathcal{O}_{8G}$ represents chromo-magnetic penguin operator. The diagram for Magnetic Penguin Operators is given in Figure (4.4).

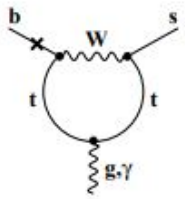

Figure 4.4: Magnetic Penguin Operators

ΔS=2 and ΔB=2 Operators

$$\mathcal{O}(\Delta S = 2) = (\overline{s}d)_{V-A}(\overline{s}d)_{V-A},$$
$$\mathcal{O}(\Delta B = 2) = (\overline{b}d)_{V-A}(\overline{b}d)_{V-A}.$$

The diagram for ΔS=2 and ΔB=2 Operators is given in Figure (4.5).

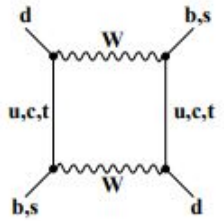

Figure 4.5: ΔS=2 and ΔB=2 Operators

Semileptonic Operators

$$\mathcal{O}_{7V} = (\overline{s}d)_{V-A}(\overline{e}e)_V,$$
$$\mathcal{O}_{7A} = (\overline{s}d)_{V-A}(\overline{e}e)_A,$$
$$\mathcal{O}_{9V} = (\overline{b}s)_{V-A}(\overline{e}e)_V,$$
$$\mathcal{O}_{10A} = (\overline{b}s)_{V-A}(\overline{e}e)_A,$$

$$\mathcal{O}(\overline{\nu}\nu) = (\overline{s}d)_{V-A}(\overline{\nu}\nu)_{V-A},$$
$$\mathcal{O}(\overline{\mu}\mu) = (\overline{s}d)_{V-A}(\overline{\mu}\mu)_{V-A}.$$

The diagram for Semileptonic Operators is given in Figure (4.6).

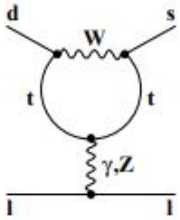

Figure 4.6: Semileptonic Operators

In the operators given above i and j refers to the color indices, q is commonly regarded as representing the up (u), down (d), strange (s), and charm (c) quarks. and $V \pm A$ is used to denote Lorentz structure $\gamma_\mu(1\pm\gamma_5)$. Therefore shorthand notation $(\overline{q}q)_{V\pm A}$ represents

$\overline{q}\gamma_\mu(1 \pm \gamma_5)q$. In FCNC $b \to d$ transition the short-range impacts are attributed to the electroweak and magnetic penguin operators whereas current-current and QCD penguin operators incorporate both short distance and long distance effects in $b \to d$ transition.

Chapter 5

The Four-Fold Angular Distribution in the Cascade Decay $B \to a_1(1260)(\to \rho\pi)l^+l^-$

In this chapter the kinematics required to study the decay $B \to a_1(\to \rho\pi)l^+l^-$ is discussed in detail, starting from the helicity formalism in the first section, next the cascade decay is discussed. Then the four-fold angular distribution and the angular coefficients are given. Then the plots for angular coefficients as function of q^2 for longitudinally and transversely polarized ρ computed within SM are also given. In last section the overview of family non-universal Z' Model is reviewed and finally expression of total Hamiltonian i.e. SM and NP Hamiltonian is given.

5.1 Helicity Formalism of the Decay $B \to a_1(\to \rho\pi)l^+l^-$ in Standard Model

To derive four-fold angular distribution for rare semileptonic decay $B \to a_1(\to \rho\pi)l^+l^-$, the complete kinematics of this decay is discussed in this section. Beginning from the effective Hamiltonian the amplitude is written. Then matrix elements and form factors are given. Next in this section the expressions of physical quantities required to study this decay are given precisely.

5.1.1 Effective Hamiltonian

The general effective Hamiltonian can be written in a form

$$\mathcal{H} = \frac{G_F}{\sqrt{2}} \sum_i V_i^{CKM} C_i(\mu) \mathcal{O}_i(\mu) \tag{5.1.1}$$

where, G_F is the Fermi coupling constant, V_i^{CKM} is the product of CKM matrix elements, $C_i(\mu)$ are the Wilson Coefficients and $\mathcal{O}_i(\mu)$ are local operators at energy scale μ governing the process under consideration i.e,

$$B \to a_1 J^\mu_{eff} \tag{5.1.2}$$

where, B is the initial state meson and a_1 and J^μ_{eff} are the final state meson and leptons respectively.

This decay's amplitude can be expressed as

$$\mathcal{M}(B \to a_1 J^\mu_{eff}) = \langle a_1 J^\mu_{eff} | \mathcal{H}_{eff} | B \rangle \tag{5.1.3}$$

Using the expression of Hamiltonian from equation (5.1.1) amplitude becomes

$$\mathcal{M}(B \to a_1 J^\mu_{eff}) = \frac{G_F}{\sqrt{2}} \sum_i V_i^{CKM} C_i(\mu) \langle a_1 J^\mu_{eff} |\ O_i(\mu) | B \rangle \tag{5.1.4}$$

The operators $\mathcal{O}_i$ are the relevant local operators given explicitly as follows:

$$\mathcal{O}_7 \propto (\bar{d}\sigma_{\mu\nu} P_R b) F^{\mu\nu} \tag{5.1.5}$$

$$\mathcal{O}_9 \propto (\bar{d}\gamma_\mu P_L b) \bar{l}\gamma^\mu l \tag{5.1.6}$$

$$\mathcal{O}_{10} \propto (\bar{d}\gamma_\mu P_L b) \bar{l}\gamma^\mu \gamma^5 l \tag{5.1.7}$$

where

$$\sigma^{\mu\nu} = \frac{\iota}{2}[\gamma^\mu, \gamma^\nu],$$
$$P_L = \frac{1}{2}(1 - \gamma_5),$$
$$P_R = \frac{1}{2}(1 + \gamma_5),$$

and $F^{\mu\nu}$ represents photon field strength tensor.

The decay $B \to a_1 J^\mu_{eff}$ takes place at quark level through $b \to d l^+ l^-$ FCNC transition. The short-distance effective Hamiltonian governing the process $b \to d l^+ l^-$ in the SM operator basis can be described as follows:

$$\mathcal{H}_{eff} = -\frac{G_F \alpha}{\sqrt{2}\pi} V_{tb} V_{td}^* [\mathcal{C}_7^{eff} \mathcal{O}_7 + \mathcal{C}_9^{eff} \mathcal{O}_9 + \mathcal{C}_{10}^{SM} \mathcal{O}_{10}] \tag{5.1.8}$$

where α represents electromagnetic coupling constant.

Putting the values of local operators from equations (5.1.5) - (5.1.7) in the effective Hamiltonian given in equation (5.1.8) gives

$$\mathcal{H}_{eff} = -\frac{G_F\alpha}{2\sqrt{2}\pi}V_{tb}V_{td}^*[\mathcal{C}_9^{eff}(\bar{d}\gamma_\mu(1-\gamma_5)b)\bar{l}\gamma^\mu l + \mathcal{C}_{10}^{SM}(\bar{d}\gamma_\mu(1-\gamma_5)b)\bar{l}\gamma^\mu\gamma^5 l - \frac{2m_b}{q^2}\mathcal{C}_7^{eff}(\bar{d}\iota\sigma_{\mu\nu}q^\nu(1+\gamma_5)b)\bar{l}\gamma^\mu l] \quad (5.1.9)$$

Considering the amplitude from equation (5.1.4) and using the expression of local operators in this amplitude results in

$$\mathcal{M}(b\to dl^+l^-) = \frac{G_F\alpha}{2\sqrt{2}\pi}V_{tb}V_{td}^*[\mathcal{C}_9^{eff}\langle a_1(k,\epsilon)|(\bar{d}\gamma_\mu(1-\gamma_5)b)|B(p)\rangle\bar{l}\gamma^\mu l + \mathcal{C}_{10}^{SM}\langle a_1(k,\epsilon)|(\bar{d}\gamma_\mu(1-\gamma_5)b)|B(p)\rangle\bar{l}\gamma^\mu\gamma^5 l - \frac{2m_b}{q^2}\mathcal{C}_7^{eff}\langle a_1(k,\epsilon)|(\bar{d}\iota\sigma_{\mu\nu}q^\nu(1+\gamma_5)b)|B(p)\rangle\bar{l}\gamma^\mu l] \quad (5.1.10)$$

In the above equation k represents momentum vector of the daughter meson a_1 and ϵ represents its polarization vector. Similarly p represents momentum vector of initial state meson B. The matrix elements appearing in the amplitude (5.1.10) are discussed in the next section.

5.1.2 Matrix Elements and Form Factors for $B \to a_1 l^+ l^-$ Transition

For $B \to a_1 l^+ l^-$ decay, the hadronic matrix elements are parameterized in relation to Lorentz invariant vector, axial vector and tensor form factors.[19]

The hadronic matrix elements can be written as

$$\langle a_1(k,\epsilon)|V_\mu|B(p)\rangle = \epsilon_\mu^*(m_B+m_{a_1})V_1(q^2) - (p+k)_\mu(\epsilon^*.q)\frac{V_2(q^2)}{m_B+m_{a_1}} - q_\mu(\epsilon^*.q)\frac{2m_{a_1}}{q^2}[V_3(q^2)-V_0(q^2)] \quad (5.1.11)$$

$$\langle a_1(k,\epsilon)|A_\mu|B(p)\rangle = \frac{2\iota\varepsilon_{\mu\nu\alpha\beta}}{m_B+m_{a_1}}\epsilon^{*\nu}p^\alpha k^\beta A(q^2) \quad (5.1.12)$$

where $V^\mu = \bar{d}\gamma^\mu b$ and $A^\mu = \bar{d}\gamma^\mu\gamma^5 b$ are the vector and axial vector currents respectively and $\epsilon^{*\nu}$ is the polarization vector of axial vector meson.

$$\langle a_1(k,\epsilon)|(\bar{d}\iota\sigma_{\mu\nu}q^\nu b)|B(p)\rangle = [(m_B^2-m_{a_1}^2)\epsilon_\mu^* - (\epsilon^*.q)(p+k)_\mu]T_2(q^2) + (\epsilon^*.q)[q_\mu - \frac{q^2}{m_B^2-m_{a_1}^2}(p+k)_\mu]T_3(q^2) \quad (5.1.13)$$

$$\langle a_1(k,\epsilon)|(\bar{d}\iota\sigma_{\mu\nu}q^\nu\gamma^5 b)|B(p)\rangle = 2\iota\varepsilon_{\mu\nu\alpha\beta}\epsilon^{*\nu}p^\alpha k^\beta T_1(q^2) \tag{5.1.14}$$

In these matrix elements V_0, V_1, V_2 and V_3 are the vector form factors. They are related as

$$V_3(q^2) = \frac{m_B + m_{a_1}}{2m_{a+1}}V_1(q^2) - \frac{m_B - m_{a_1}}{2m_{a+1}}V_2(q^2), \tag{5.1.15}$$

$$V_3(0) = V_0(0). \tag{5.1.16}$$

$A(q^2)$ represents the axial vector form factor and T_1, T_2 and T_3 are tensor form factors. The form factors depend on the square momentum transfer q^2 and can be extrapolated as

$$F_k(q^2) = \frac{F_k(0)}{1 - \alpha s + \beta s^2} \tag{5.1.17}$$

where $s = q^2$ and $F_k(q^2)$ are vector $V_i(q^2)$ $(i = 0, 1, 2)$, axial vector $A(q^2)$ and tensor form factors $T_j(q^2)$ $(j = 1, 2, 3)$. The calculation of form factors is carried out within framework of Light Cone Sum Rules.[20]

The numerical values of these form factors and parameters α and β can be found in appendix.

5.1.3 Kinematics

In rest frame of decaying B meson, the 4-momentum of B, a_1 and J_μ^{eff} are defined as

$$p^\mu = (m_B, 0, 0, 0)$$
$$k^\mu = (E_V, 0, 0, -\vec{k})$$
$$q^\mu = (q_0, 0, 0, \vec{k})$$

respectively. The combined 4-momentum of B and a_1 can be written as

$$P^\mu = (m_B + E_V, 0, 0, -\vec{k})$$

where

$$q_0 = \frac{m_B^2 - m_V^2 + s}{2m_B},$$
$$E_V = \frac{m_B^2 + m_V^2 - s}{2m_B},$$
$$\vec{k} = \sqrt{E_V^2 - m_V^2}.$$

Polarization vectors of hadronic current are defined as

$$\epsilon^\mu(0) = \frac{1}{\sqrt{s}}(\vec{k}, 0, 0, q_0),$$
$$\epsilon^\mu(\pm) = \frac{1}{\sqrt{2}}(0, \mp 1, -\iota, 0),$$
$$\epsilon^\mu(t) = \frac{1}{\sqrt{s}}(q_0, 0, 0, \vec{k}).$$

Polarization vectors of a_1 meson in B-rest frame are defined as

$$\epsilon_A^\mu(0) = \frac{1}{m_V}(\vec{k}, 0, 0, -E_V),$$
$$\epsilon_A^\mu(\pm) = \frac{1}{\sqrt{2}}(0, \pm 1, -\iota, 0).$$

5.1.4 Hadron Helicity Amplitude

The amplitude for hadronic current produced in decay $B \to a_1 l^+ l^-$ in helicity basis can be expressed as

$$H_{11}(i,j) = H_1(i)H_1^\dagger(j),$$
$$H_{22}(i,j) = H_2(i)H_2^\dagger(j),$$
$$H_{12}(i,j) = H_1(i)H_2^\dagger(j),$$
$$H_{21}(i,j) = H_2(i)H_1^\dagger(j).$$

where

$$H_1(i) = -\iota\mathcal{F}_1 \sum_{\mu=0}^{3}\sum_{\nu=0}^{3}\sum_{\alpha=0}^{3}\sum_{\beta=0}^{3} \epsilon_{\mu\nu\alpha\beta}\epsilon^{\mu\dagger}(i)\epsilon^{\nu\dagger}(i)p^\alpha k^\beta - \mathcal{F}_2(\epsilon^{\mu\dagger}(i).\epsilon_{\mu V}^\dagger(i)) + \mathcal{F}_3(\epsilon^{\mu\dagger}(i).P_\mu)(\epsilon_V^{\mu\dagger}(i).q_\mu) + \mathcal{F}_4(\epsilon^{\mu\dagger}(i).q_\mu)(\epsilon_V^{\mu\dagger}(i).q_\mu). \quad (5.1.18)$$

$$H_2(i) = -\iota\mathcal{F}_5 \sum_{\mu=0}^{3}\sum_{\nu=0}^{3}\sum_{\alpha=0}^{3}\sum_{\beta=0}^{3} \epsilon_{\mu\nu\alpha\beta}\epsilon^{\mu\dagger}(i)\epsilon^{\nu\dagger}(i)p^\alpha k^\beta - \mathcal{F}_6(\epsilon^{\mu\dagger}(i).\epsilon_{\mu V}^\dagger(i)) + \mathcal{F}_7(\epsilon^{\mu\dagger}(i).P_\mu)(\epsilon_V^{\mu\dagger}(i).q_\mu) + \mathcal{F}_8(\epsilon^{\mu\dagger}(i).q_\mu)(\epsilon_V^{\mu\dagger}(i).q_\mu). \quad (5.1.19)$$

$H_1^\dagger(j)$ and $H_2^\dagger(j)$ are complex conjugates of $H_1(i)$ and $H_2(i)$ respectively.

$\mathcal{F}_1$ to $\mathcal{F}_8$ are the auxiliary functions. They contain Wilson Coefficients and form factors.

They are defined as

$$\mathcal{F}_1 = 2(C_9^{eff} + C_9^{NP} - C_9')\frac{A(q^2)}{m_B + m_{a_1}} + \frac{4m_b}{q^2}(C_7^{eff} + C_7^{NP} - C_7')T_1(q^2)$$

$$\mathcal{F}_2 = 2(C_9^{eff} + C_9^{NP} + C_9')(m_B + m_{a_1})V_1(q^2) - \frac{2m_b}{q^2}(C_7^{eff} + C_7^{NP} + C_7')(m_B^2 - m_{a_1}^2)T_2(q^2)$$

$$\mathcal{F}_3 = (C_9^{eff} + C_9^{NP} + C_9')\frac{2m_b}{q^2}[V_3(q^2) - V_0(q^2)] + \frac{2m_b}{q^2}(C_7^{eff} + C_7^{NP} + C_7')T_3(q^2)$$

$$\mathcal{F}_4 = (C_9^{eff} + C_9^{NP} + C_9')\frac{V_2(q^2)}{m_B + m_{a_1}} - \frac{2m_b}{q^2}(C_7^{eff} + C_7^{NP} + C_7')T_2(q^2)$$
$$- \frac{2m_b}{q^2}(C_7^{eff} + C_7^{NP} + C_7')\frac{q^2}{m_B^2 - m_{a_1^2}}T_3(q^2)$$

$$\mathcal{F}_5 = 2(C_{10}^{SM} + C_{10}^{NP} - C_{10}')\frac{A(q^2)}{m_B + m_{a_1}}$$

$$\mathcal{F}_6 = 2(C_{10}^{SM} + C_{10}^{NP} + C_{10}')(m_B + m_{a_1})V_1(q^2)$$

$$\mathcal{F}_7 = (C_{10}^{SM} + C_{10}^{NP} + C_{10}')\frac{2m_{a_1}}{q^2}[V_3(q^2) - V_0(q^2)]$$

$$\mathcal{F}_8 = (C_{10}^{SM} + C_{10}^{NP} + C_{10}')\frac{V_2(q^2)}{m_B + m_{a_1}}$$

In the above equations C_7^{eff}, C_9^{eff} and C_{10}^{SM} are the Standard Model Wilson Coefficients where as $C_7^{NP}, C_7', C_9^{NP}, C_9'$ and C_{10}^{NP}, C_{10}' are the New Physics Wilson Coefficients. NP Wilson Coefficients appear in New Physics amplitude are given in Section (5.4).

5.1.5 Lepton Helicity Amplitude

The amplitude for leptonic part (effective current) produced in decay $B \to a_1 l^+ l^-$ in helicity basis can be written as

$$L_{mn}(i,j) = -4m^2(\epsilon_l^\mu(i).\epsilon_{\mu l}^\dagger(j)) - 4(\epsilon_l^\mu(i).\epsilon_{\mu l}^\dagger(j))(p_1^\mu.p_{2\mu}) + 4(p_1^\mu.\epsilon_{\mu l}(i))(p_2^\mu.\epsilon_{\mu l}^\dagger(j)) + 4(p_2^\mu.\epsilon_{\mu l}(i))(p_1^\mu.\epsilon_{\mu l}^\dagger(j)) \quad (5.1.20)$$

with m=n=1,2 and

$$L_{mn}(i,j) = 4\iota \sum_{\mu=0}^{3}\sum_{\nu=0}^{3}\sum_{\alpha=0}^{3}\sum_{\beta=0}^{3} \epsilon^{\mu\nu\alpha\beta}\epsilon_{l\mu}(i).\epsilon_{\nu l}^\dagger(j)p_{1\alpha}.p_{2\beta} \quad (5.1.21)$$

with $m \neq n$ and $i, j = 0, \pm, t$ correspond to longitudinal, transverse and time-like polarizations. p_1^μ and p_2^μ are the 4-momenta of l^+ and l^- respectively.

In the rest frame of B meson, the energy and momentum vectors of the leptons are

defined as follows

$$\mathcal{E}_1 = \frac{\sqrt{s}}{2}$$
$$|\vec{p}_1| = \frac{\sqrt{s-4m^2}}{2}$$

The 4-momenta of l^+ and l^- are defined as

$$p_1^\mu = (\mathcal{E}_1, |\vec{p}_1|\sin\theta\cos\chi, |\vec{p}_1|\sin\theta\sin\chi, |\vec{p}_1|\cos\theta),$$
$$p_2^\mu = (\mathcal{E}_1, -|\vec{p}_1|\sin\theta\cos\chi, -|\vec{p}_1|\sin\theta\sin\chi, -|\vec{p}_1|\cos\theta).$$

The polarization vectors of effective current are given as

$$\epsilon_l^\mu(0) = (0,0,0,1),$$
$$\epsilon_l^\mu(\pm) = \frac{1}{\sqrt{2}}(0, \mp 1, -\iota, 0),$$
$$\epsilon_l^\mu(t) = (1,0,0,0).$$

The polarization vectors satisfy orthonormality and completeness relations:

$$\epsilon_l^{\mu\dagger}(a)\epsilon_{l\mu}(b) = g_{ab},$$
$$\epsilon_l^{\mu}(a)\epsilon_l^{\nu\dagger}(b)\delta_{ab} = g^{\mu\nu}.$$

5.2 Cascade Decay $a_1 \to \rho\pi$

The daughter meson a_1 produced in decay $B \to a_1 l^+ l^-$ subsequently decays to $\rho\pi$. The decay mode $a_1 \to \rho\pi$ can be parameterized by matrix element as

$$\mathcal{A}(a_1(k^\mu) \to \rho(p_V^\mu)\pi(p_S^\mu)) = \frac{-2g_{a_1\rho\pi}}{m_{a_1}m_\rho}\Big[(k^\mu.p_{V\mu})(\epsilon_{a_1\mu}(i).\epsilon_\rho^{\mu\dagger}(j)) - (p_V^\mu.\epsilon_{a_1\mu}(i))(k_\mu.\epsilon_\rho^{\mu\dagger}(j))\Big] \tag{5.2.1}$$

where $i,j = 0,\pm$ corresponds to longitudinal and transverse polarizations. k, ϵ_{a_1} and p_V, ϵ_ρ are momentum and polarization vectors of a_1 and ρ respectively.

In rest frame of a_1 meson, energy and momentum vector of ρ meson are defined as

$$\mathcal{E}_\rho = \sqrt{m_\rho^2 + |\vec{p}_3|}$$
$$|\vec{p}_3| = \frac{\sqrt{\lambda(m_{a_1}^2, m_\rho^2, m_\pi^2)}}{2m_{a_1}}$$

where $\lambda(m_{a_1}^2, m_\rho^2, m_\pi^2)$ is the shallon function. It is defined as

$$\lambda(m_{a_1}^2, m_\rho^2, m_\pi^2) = m_{a_1}^4 + m_\rho^4 + m_\pi^4 - 2m_{a_1}m_\rho - 2m_{a_1}m_\pi - 2m_\rho m_\pi$$

The 4-momenta of a_1, ρ and π mesons are defined as

$$\begin{aligned} k^\mu &= (m_{a_1}, \vec{0}), \\ p_V^\mu &= (\mathcal{E}_\rho, |\vec{p}_3|\sin\theta_V, 0, -|\vec{p}_3|\cos\theta_V), \\ p_S^\mu &= (\mathcal{E}_S, -|\vec{p}_3|\sin\theta_V, 0, |\vec{p}_3|\cos\theta_V). \end{aligned}$$

respectively. $\mathcal{E}_\rho$ and $\mathcal{E}_S$ are the energies of ρ and π mesons respectively.

The polarization vectors of a_1 and π mesons in rest frame of a_1 are given by

$$\begin{aligned} \epsilon_{a_1}^\mu(\pm) &= \frac{1}{\sqrt{2}}(0, \pm 1, -\iota, 0), \\ \epsilon_{a_1}^\mu(0) &= \frac{1}{\sqrt{2}}(0, 0, 0, -1), \\ \epsilon_V^\mu(\pm) &= \frac{1}{\sqrt{2}}(0, \cos\theta_V, \mp\iota, \sin\theta_V), \\ \epsilon_V^\mu(0) &= \frac{1}{m_\rho}(\vec{p}_3, \mathcal{E}_\rho\sin\theta_V, 0, -\mathcal{E}_\rho\cos\theta_V). \end{aligned}$$

The relative configuration of $(\rho\pi)-$ and $(l^+l^-)-$ planes and definition of decay angles are shown in Figure (5.1).

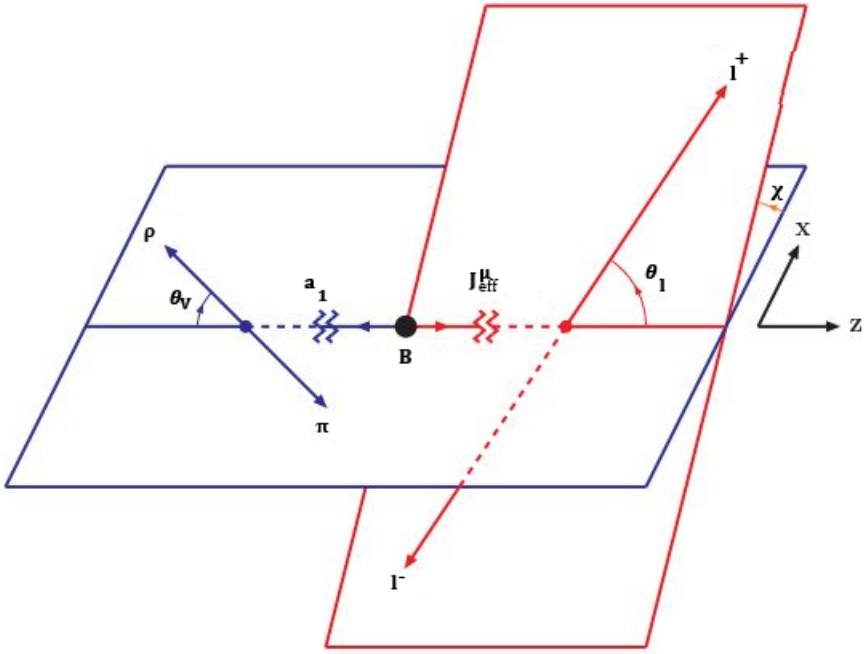

Figure 5.1: Kinematics of decay mode $B \to a_1(\to \rho\pi)l^+l^-$

5.3 Family Non-Universal Z' Model

By adding an extra symmetry gauge group $U(1)'$ in SM we get a massive, neutral gauge boson known as Z'.In the family non-universal Z' model, the occurrence of tree-level flavor-changing neutral current (FCNC) transitions in the $b \to d$ process is attributed to the presence of a non-diagonal chiral coupling matrix. [21, 22]

In the context of the family non-universal Z' model, the effective Hamiltonian describing the rare semileptonic decay $b \to dl^+l^-$ can be formulated as

$$\mathcal{H}_{eff}^{Z'} = -\frac{4G_F}{\sqrt{2}} V_{tb}V_{td}^*[\Lambda_{db}\mathcal{C}_9^{Z'}\mathcal{O}_9 + \Lambda_{db}\mathcal{C}_{10}^{Z'}\mathcal{O}_{10}] \tag{5.3.1}$$

where

$$\Lambda_{db} = \frac{4\pi e^{-\iota\phi_{db}}}{\alpha V_{tb}V_{td}^*}$$

$\mathcal{C}_9^{Z'}$ and $\mathcal{C}_{10}^{Z'}$ are the modified Wilson coefficients in which NP effects arises whereas $\mathcal{O}_9$ and $\mathcal{O}_{10}$ are the same SM operators. The modification in Wilson coefficients occur due to the off-diagonal interactions between quarks and leptons with Z' gauge boson. These

Wilson coefficients are defined as

$$\mathcal{C}_9^{Z'} = |B_{db}^L||S_{LR}|;$$
$$\mathcal{C}_{10}^{Z'} = |B_{db}^L||D_{LR}|$$

where

$$|S_{LR}| = B_{ll}^L + B_{ll}^R$$
$$|D_{LR}| = B_{ll}^L - B_{ll}^R$$

S_{LR} and D_{LR} incorporate the couplings between new Z' gauge boson and left and right handed leptons. Furthermore $B_{db}^L = |B_{db}^L|e^{\iota\phi_{db}}$ is the left handed coupling between quarks and Z' gauge boson and ϕ_{db} represents the new CP-violating phase which is absent in the SM.

Finally, the total amplitude for the decay $B \to a_1 l^+ l^-$ includes both SM as well as Z' model amplitude. It can be written as

$$\mathcal{M}^{tot} = \mathcal{M}^{SM} + \mathcal{M}^{Z'} \tag{5.3.2}$$

Similarly the total Wilson coefficients can be written as

$$\mathcal{C}_9^{tot} = \mathcal{C}_9^{eff} + \Lambda_{db}\mathcal{C}_9^{Z'} \tag{5.3.3}$$
$$\mathcal{C}_{10}^{tot} = \mathcal{C}_{10}^{SM} + \Lambda_{db}\mathcal{C}_{10}^{Z'}. \tag{5.3.4}$$

The total Hamiltonian can be written as

$$\mathcal{H}^{tot} = \mathcal{H}_{eff} + \mathcal{H}_{eff}^{Z'} \tag{5.3.5}$$

where $\mathcal{H}_{eff}$ is given in equation (5.1.11) and $\mathcal{H}_{eff}^{Z'}$ can be written as

$$\begin{aligned}\mathcal{H}_{eff}^{Z'} = -\frac{G_F\alpha}{2\sqrt{2}\pi}V_{tb}V_{td}^*[&\mathcal{C}_9^{NP}\langle a_1(k,\epsilon)|(\bar{d}\gamma_\mu(1-\gamma_5)b)|B(p)\rangle\bar{l}\gamma^\mu l + \mathcal{C}_9'\langle a_1(k,\epsilon)|(\bar{d}\gamma_\mu(1+\gamma_5)b)|B(p)\rangle\bar{l}\gamma^\mu l \\ &+ \mathcal{C}_{10}^{NP}\langle a_1(k,\epsilon)|(\bar{d}\gamma_\mu(1-\gamma_5)b)|B(p)\rangle\bar{l}\gamma^\mu\gamma^5 l + \mathcal{C}_{10}'\langle a_1(k,\epsilon)|(\bar{d}\gamma_\mu(1+\gamma_5)b)|B(p)\rangle\bar{l}\gamma^\mu\gamma^5 l \\ -\frac{2m_b}{q^2}\mathcal{C}_7^{NP}\langle a_1(k,\epsilon)|(\bar{d}\iota\sigma_{\mu\nu}q^\nu(1+\gamma_5)b)|B(p)\rangle\bar{l}\gamma^\mu l &- \frac{2m_b}{q^2}\mathcal{C}_7'\langle a_1(k,\epsilon)|(\bar{d}\iota\sigma_{\mu\nu}q^\nu(1-\gamma_5)b)|B(p)\rangle\bar{l}\gamma^\mu l]\end{aligned} \tag{5.3.6}$$

In terms of NP Wilson Coefficients and local operators total Hamiltonian can be written as

$$\mathcal{H}_{eff} = -\frac{G_F\alpha}{2\sqrt{2}\pi}V_{tb}V_{td}^*[(\mathcal{C}_9^{eff} + \mathcal{C}_9^{NP})\langle a_1(k,\epsilon)|(\bar{d}\gamma_\mu(1-\gamma_5)b)|B(p)\rangle\bar{l}\gamma^\mu l + \mathcal{C}_9'\langle a_1(k,\epsilon)|(\bar{d}\gamma_\mu(1+\gamma_5)b)|B(p)\rangle\bar{l}\gamma^\mu l (\mathcal{C}_{10}^{SM}+\mathcal{C}_{10}^{NP})\langle a_1(k,\epsilon)|(\bar{d}\gamma_\mu(1-\gamma_5)b)|B(p)\rangle\bar{l}\gamma^\mu\gamma^5 l+\mathcal{C}_{10}'\langle a_1(k,\epsilon)|(\bar{d}\gamma_\mu(1+\gamma_5)b)|B(p)\rangle\bar{l}\gamma^\mu\gamma^5 l - \frac{2m_b}{q^2}(\mathcal{C}_7^{eff} + \mathcal{C}_7^{NP})\langle a_1(k,\epsilon)|(\bar{d}\imath\sigma_{\mu\nu}q^\nu(1+\gamma_5)b)|B(p)\rangle\bar{l}\gamma^\mu l - \frac{2m_b}{q^2}\mathcal{C}_7'\langle a_1(k,\epsilon)|(\bar{d}\imath\sigma_{\mu\nu}q^\nu(1-\gamma_5)b)|B(p)\rangle\bar{l}\gamma^\mu l] \quad (5.3.7)$$

5.4 Angular Decay Distribution

The decay $B \to a_1(\to \rho\pi)l^+l^-$ is mediated at quark level through $b \to d$ transition and therefore account for FCNC process. In SM, FCNC transitions are forbidden at tree level, however these decays are mediated by higher order penguin diagrams.

The angular configuration of $\rho\pi l^+l^-$ system is characterized by the decay angles θ, θ_V and χ. In this context, θ and θ_V denote the angles of the $\rho\pi(l^+l^-)$ relative to the flight direction of B meson in the $\rho\pi(l^+l^-)$ centre-of-mass frame respectively. The χ denotes the relative orientation of the $\rho\pi$ and l^+l^- decay planes in the centre-of-mass frame of B meson.

5.4.1 Differential Decay Distribution

One can express the differential decay distribution for a longitudinally polarized ρ in the following form.

$$\frac{d^4\Gamma_\parallel}{dq^2 d\theta d\theta_V d\chi} = \frac{9}{32\pi}\mathcal{N}_\parallel I_\parallel(q^2,\theta,\theta_V,\chi) \quad (5.4.1)$$

where

$$I_\parallel(q^2,\theta,\theta_V,\chi) = I_{1s,\parallel}\sin^2\theta_V + I_{1c,\parallel}\cos^2\theta_V + I_{2s,\parallel}\sin^2\theta_V\cos(2\theta) + I_{2c,\parallel}\cos^2\theta_V\cos(2\theta) + I_{3,\parallel}\sin^2\theta_V\sin^2\theta\cos(2\chi) + I_{4,\parallel}\sin(2\theta_V)\sin(2\theta)\cos\chi + I_{5,\parallel}\sin(2\theta_V)\sin\theta\cos\chi + I_{6s,\parallel}\sin^2\theta_V\cos\theta + I_{6c,\parallel}\cos^2\theta_V\cos\theta + I_{7,\parallel}\sin(2\theta_V)\sin\theta\sin\chi + I_{8,\parallel}\sin(2\theta_V)\sin(2\theta)\sin\chi + I_{9,\parallel}\sin^2\theta_V\sin^2\theta\sin(2\chi)$$

One can express the differential decay distribution for a transversely polarized ρ in the following form.

$$\frac{d^4\Gamma_\perp}{dq^2 d\theta d\theta_V d\chi} = \frac{9}{32\pi}\mathcal{N}_\perp I_\perp(q^2, \theta, \theta_V, \chi) \tag{5.4.2}$$

where

$$I_\perp(q^2,\theta,\theta_V,\chi) = I_{1s,\perp}\sin^2\theta_V + I_{1c,\perp}\cos^2\theta_V + I_{2s,\perp}\sin^2\theta_V\cos(2\theta) + I_{2c,\perp}\cos^2\theta_V\cos(2\theta)$$
$$+ I_{3,\perp}\sin^2\theta_V\sin^2\theta\cos(2\chi) + I_{4,\perp}\sin(2\theta_V)\sin(2\theta)\cos\chi + I_{5,\perp}\sin(2\theta_V)\sin\theta\cos\chi$$
$$+ I_{6s,\perp}\sin^2\theta_V\cos\theta + I_{6c,\perp}\cos^2\theta_V\cos\theta + I_{7,\perp}\sin(2\theta_V)\sin\theta\sin\chi$$
$$+ I_{8,\perp}\sin(2\theta_V)\sin(2\theta)\sin\chi + I_{9,\perp}\sin^2\theta_V\sin^2\theta\sin(2\chi)$$

and $\mathcal{N}_\parallel$ and $\mathcal{N}_\perp$ contains the constant terms. They are expressed as

$$\mathcal{N}_\parallel = V_{tb}V_{td}^*\left[\frac{G_F^2\alpha^2}{3.2^{10}\pi^5 m_B^3}q^2\sqrt{\lambda}\beta\right]^{\frac{1}{2}}\mathcal{B}(a_1 \to \rho_\parallel\pi) \tag{5.4.3}$$

and

$$\mathcal{N}_\perp = V_{tb}V_{td}^*\left[\frac{G_F^2\alpha^2}{3.2^{10}\pi^5 m_B^3}q^2\sqrt{\lambda}\beta\right]^{\frac{1}{2}}\mathcal{B}(a_1 \to \rho_\perp\pi) \tag{5.4.4}$$

with $\lambda \equiv \lambda(m_B^2, m_{a_1}^2, q^2)$, $\beta = \sqrt{1-\frac{4m^2}{q^2}}$ and m represents the mass of lepton.

In above equations $I_\parallel$ and $I_\perp$ are angular coefficient functions for longitudinally and transversely polarized ρ respectively. The expressions and plots for these angular coefficients are given in the next section. Since,

$$\Gamma = \Gamma_\parallel + \Gamma_\perp \tag{5.4.5}$$

Hence, the overall decay distribution can be expressed as

$$\frac{d^4\Gamma}{dq^2 d\theta d\theta_V d\chi} = \frac{d^4\Gamma_\parallel}{dq^2 d\theta d\theta_V d\chi} + \frac{d^4\Gamma_\perp}{dq^2 d\theta d\theta_V d\chi} \tag{5.4.6}$$

In terms of I's it is written as

$$\frac{d^4\Gamma}{dq^2 d\theta d\theta_V d\chi} = \frac{9}{32\pi}[\mathcal{N}_\parallel I_\parallel(q^2,\theta,\theta_V,\chi) + \mathcal{N}_\perp I_\perp(q^2,\theta,\theta_V,\chi)] \tag{5.4.7}$$

Putting the expressions of $I_\parallel$ and $I_\perp$ in the above equation leads to

$$\frac{d^4\Gamma}{dq^2 d\theta d\theta_V d\chi} = \frac{9}{32\pi}[\mathcal{N}_\parallel(I_{1s,\parallel}\sin^2\theta_V + I_{1c,\parallel}\cos^2\theta_V + I_{2s,\parallel}\sin^2\theta_V\cos(2\theta)$$
$$+ I_{2c,\parallel}\cos^2\theta_V\cos(2\theta) + I_{3,\parallel}\sin^2\theta_V\sin^2\theta\cos(2\chi) + I_{4,\parallel}\sin(2\theta_V)\sin(2\theta)\cos\chi$$
$$+ I_{5,\parallel}\sin(2\theta_V)\sin\theta\cos\chi + I_{6s,\parallel}\sin^2\theta_V\cos\theta + I_{6c,\parallel}\cos^2\theta_V\cos\theta + I_{7,\parallel}\sin(2\theta_V)\sin\theta\sin\chi$$
$$+ I_{8,\parallel}\sin(2\theta_V)\sin(2\theta)\sin\chi + I_{9,\parallel}\sin^2\theta_V\sin^2\theta\sin(2\chi)) + \mathcal{N}_\perp(I_{1s,\perp}\sin^2\theta_V$$
$$+ I_{1c,\perp}\cos^2\theta_V + I_{2s,\perp}\sin^2\theta_V\cos(2\theta) + I_{2c,\perp}\cos^2\theta_V\cos(2\theta) + I_{3,\perp}\sin^2\theta_V\sin^2\theta\cos(2\chi)$$
$$+ I_{4,\perp}\sin(2\theta_V)\sin(2\theta)\cos\chi + I_{5,\perp}\sin(2\theta_V)\sin\theta\cos\chi + I_{6s,\perp}\sin^2\theta_V\cos\theta + I_{6c,\perp}\cos^2\theta_V\cos\theta$$
$$+ I_{7,\perp}\sin(2\theta_V)\sin\theta\sin\chi + I_{8,\perp}\sin(2\theta_V)\sin(2\theta)\sin\chi + I_{9,\perp}\sin^2\theta_V\sin^2\theta\sin(2\chi))]$$

5.4.2 Angular Coefficients

Angular Coefficients are coefficients of combinations of trigonometric functions that describe the planes in coordinate system assigned to decay $B \to a_1(\to \rho\pi)l^+l^-$. These coefficients are represented using hadronic matrix elements. The parallel and perpendicular angular coefficients corresponds to longitudinally and transversely polarized ρ respectively. The expressions for these coefficients are given below.

Parallel Angular Coefficients

$$I_{1s,\parallel} = \frac{(\beta^2+2)}{2}(|H_+^1|^2 + |H_-^1|^2 + |H_+^2|^2 + |H_-^2|^2) + \frac{4m^2}{s}(|H_+^1|^2 + |H_-^1|^2 - |H_+^2|^2 - |H_-^2|^2)$$
$$I_{1c,\parallel} = \frac{8m^2}{s}(|H_0^1|^2 - |H_0^2|^2 + 2|H_t^2|^2) + 2(|H_0^1|^2 + |H_0^2|^2)$$
$$I_{2s,\parallel} = \frac{\beta^2}{2}(|H_+^1|^2 + |H_-^1|^2 + |H_+^2|^2 + |H_-^2|^2)$$
$$I_{2c,\parallel} = -2\beta^2(|H_0^1|^2 + |H_0^2|^2)$$
$$I_{3,\parallel} = -2\beta^2(H_+^1 H_-^{1*} + H_+^2 H_-^{2*})$$
$$I_{4,\parallel} = \beta^2(H_+^1 H_0^{1*} + H_-^1 H_0^{1*} + H_+^2 H_0^{2*} + H_-^2 H_0^{2*})$$
$$I_{5,\parallel} = -2\beta(H_+^1 H_0^{2*} - H_-^1 H_0^{2*} + H_+^2 H_0^{1*} - H_-^2 H_0^{1*})$$
$$I_{6s,\parallel} = -4\beta(H_+^1 H_+^{2*} - H_-^1 H_-^{2*})$$
$$I_{6c,\parallel} = 0$$
$$I_{7,\parallel} = -2\iota\beta(H_0^1 H_+^{2*} + H_0^1 H_-^{2*} + H_0^2 H_+^{1*} + H_0^2 H_-^{1*})$$
$$I_{8,\parallel} = \iota\beta^2(H_0^1 H_+^{1*} - H_0^1 H_-^{1*} + H_0^2 H_+^{2*} - H_0^2 H_-^{2*})$$
$$I_{9,\parallel} = 2\iota\beta^2(H_+^1 H_-^{1*} + H_+^2 H_-^{2*})$$

Perpendicular Angular Coefficients

$$I_{1s,\perp} = \frac{(\beta^2+2)}{4}(|H_+^1|^2 + |H_-^1|^2 + |H_+^2|^2 + |H_-^2|^2) + (|H_0^1|^2 + |H_0^2|^2)$$
$$+ \frac{2m^2}{s}[(|H_+^1|^2 + |H_-^1|^2 - |H_+^2|^2 - |H_-^2|^2) + (|H_0^1|^2 - |H_0^2|^2 + 2|H_t^2|^2)]$$
$$I_{1c,\perp} = \frac{(\beta^2+2)}{2}(|H_+^1|^2 + |H_-^1|^2 + |H_+^2|^2 + |H_-^2|^2) + \frac{4m^2}{s}(|H_+^1|^2 + |H_-^1|^2 - |H_+^2|^2 - |H_-^2|^2)$$
$$I_{2s,\perp} = -\beta^2[(|H_0^1|^2 + |H_0^2|^2) - \frac{1}{4}(|H_+^1|^2 + |H_-^1|^2 + |H_+^2|^2 + |H_-^2|^2)]$$
$$I_{2c,\perp} = \frac{\beta^2}{2}(|H_+^1|^2 + |H_-^1|^2 + |H_+^2|^2 + |H_-^2|^2)$$
$$I_{3,\perp} = \beta^2(H_+^1 H_-^{1*} + H_+^2 H_-^{2*})$$
$$I_{4,\perp} = -\frac{\beta^2}{2}(H_+^1 H_0^{1*} + H_-^1 H_0^{1*} + H_+^2 H_0^{2*} + H_-^2 H_0^{2*})$$
$$I_{5,\perp} = \beta(H_+^1 H_0^{2*} - H_-^1 H_0^{2*} + H_+^2 H_0^{1*} - H_-^2 H_0^{1*})$$
$$I_{6s,\perp} = -4\beta(H_+^1 H_+^{2*} - H_-^1 H_-^{2*} + H_+^2 H_+^{1*} - H_-^2 H_-^{1*})$$
$$I_{6c,\perp} = -8\beta(H_+^1 H_+^{2*} - H_-^1 H_-^{2*} + H_+^2 H_+^{1*} - H_-^2 H_-^{1*})$$
$$I_{7,\perp} = \iota\beta(H_0^1 H_+^{2*} + H_0^1 H_-^{2*} + H_0^2 H_+^{1*} + H_0^2 H_-^{1*})$$
$$I_{8,\perp} = \frac{\iota\beta^2}{2}(H_0^1 H_+^{1*} - H_0^1 H_-^{1*} + H_0^2 H_+^{2*} - H_0^2 H_-^{2*})$$
$$I_{9,\perp} = -\iota\beta^2(H_+^1 H_-^{1*} + H_+^2 H_-^{2*})$$

Chapter 6

Angular Analysis of Physicsl Observables of $B \to a_1(1260)(\to \rho\pi)l^+l^-$ Decay in Standard and Family Non-Universal Z' Model

This chapter is dedicated to results and discussion of the physical observables that are computed for decay $B \to a_1(\to \rho\pi)l^+l^-$ in Standard Model and Scenario 1 and Scenario 2 of family non-universal Z' Model. In first section the plots of angular coefficients $I_i(q^2)$ as a function of q^2 for longitudinally and transversely polarized ρ are plotted within SM as well as in family non universal Z' model for Scenario 1 and Scenario 2 are given and analyzed in detail. In next sections the expressions of physical observables such as branching ratio, FBA computed in terms of angular coefficients, within SM and both scenarios of Z' model are given and discussed. Also these observables are compared between SM and both scenarios of Z' Model. Furthermore the plots of above mentioned observables are also given and discussed in detail.

6.1 Comparison of Angular Coefficient Functions in Standard and Z' Model

The coefficient of $\sin(2\theta_V)\sin\theta\sin\chi$ in decay distribution represented as $I_{7,(\parallel,\perp)}$ plotted in SM and two scenarios of Z' has shown significant deviation in Z' scenario 2 from SM and Z' scenario 1, can be clearly seen in plots in Figures (6.1) and (6.2) for longitudinal and transverse polarizations respectively. It is a clear indication and provides confidence that Z' model can explain the searches beyond SM. The expressions of angular coefficients in SM are given in Section (5.3.2).

$I_{1s,\parallel}$ is same as $I_{1c,\perp}$. The SM and Z' scenario 1 values almost coincides except for just a small range of q^2 values i.e. $q^2 = (1 \text{ to } 3)$ GeV^2 where SM values are greater than Z' scenario 1 values. Similarly SM and Z' scenario 2 values coincides again except for small range of q^2 values i.e. $q^2 = (4 \text{ to } 8)$ GeV^2 where SM values are greater than Z' scenario 2 values. While comparing the Z' scenarios, it is observed that for smaller values of q^2 S2 has higher values than S1 whereas for larger values of q^2 S1 has higher values than S2.

In $I_{1s,\perp}$, the SM and Z' S1 values coincides at almost all range except only for a small range i.e. $q^2 = (0.5 \text{ to } 3)$ GeV^2 where SM values are little lower than Z' S1 values whereas the SM and Z' S2 coincides at all range of q^2. For the range $q^2 = (3 \text{ to } 15)$ GeV^2, the values computed in Z' S1 are lower than the values computed in Z' S2.

In $I_{1c,\parallel}$, the SM and Z' S1 values almost coincides except for a small range of q^2 values i.e. $q^2 = (1-4)$ GeV^2 where S1 values are higher than SM values. SM and Z' S2 values also coincides except for a small q^2 range i.e. $q^2 = (3-7)$ GeV^2 where Z' S2 values are slightly higher than SM values. While comparing the Z' scenarios, it is observed that for smaller values of q^2 S1 has higher values than S2 whereas for larger values of q^2 S2 has higher values than S1.

$I_{2s,\parallel}$ and $I_{2c,\perp}$ are same. In both cases the SM and Z' S1 values deviate in a small range of q^2 values i.e. $q^2 = (1-3)$ GeV^2 where SM values are higher than Z' S1 values. The SM and Z' S2 values also deviate slightly in q^2 region from $q^2 = 3$ GeV^2 to $q^2 = 7$ GeV^2. In Z' scenarios, from $q^2 = 0$ GeV^2 to $q^2 = 1$ GeV^2, S1 values are less than S2 values. In the range $q^2 = (1-3)$ GeV^2 both S1 and S2 values coincide in the region $q^2 > 3$ GeV^2 the S1 values are higher than S2 values.

In $I_{2s,\perp}$, the SM and Z' S1 values coincides at all range of q^2 except for small range i.e. q^2= (1 to 3) GeV^2 where SM values are greater than Z' S1 values and same is the case for SM and Z' S2 values where the deviation range is q^2= (3 to 8) GeV^2. For the range of q^2= (3 to 15) GeV^2 S1 values are greater than S2 values.

In $I_{2c,\parallel}$, SM and Z' S1 values coincide at all range of q^2 values except for a very small range i.e. $q^2 = (1-2)$ GeV^2 where SM values are slightly higher than Z' S1 values. Similarly SM and Z' S2 values coincides at all range of q^2 again except for a small range i.e. $q^2 = (3-7)$ GeV^2 where SM values are slightly higher than Z' S2 values. Comparing Z' scenarios, for smaller range of q^2 values both scenarios coincide and for larger values of q^2 Z' S1 has higher values than Z' S2.

In $I_{3,(\parallel,\perp)}$ and $I_{4,(\parallel,\perp)}$, the SM and Z' S1 values coincide at all range of q^2 values whereas Z' S2 values deviate from SM values in the range $q^2 = (3-10)$ GeV^2 where Z' S2 values are higher than SM values for $I_{3,\parallel}$ and $I_{4,\perp}$ and lower than SM values for $I_{3,\perp}$ and $I_{4,\parallel}$. While comparing Z' S1 and S2, for $I_{3,\parallel}$ and $I_{4,\perp}$ the S2 values are higher than S1 values and for $I_{3,\perp}$ and $I_{4,\parallel}$ the S1 values are higher than S2 values at all range of q^2.

In $I_{5,\parallel}$ and $I_{6s,\parallel}$, the SM values are higher than Z' S1 values in the range $q^2 = (1-6)$ GeV^2 whereas SM and Z' S2 values coincide completely at all range of q^2. The S1 values are lower than S2 values in the range $q^2 = (0-8)$ GeV^2 for $I_{5,\parallel}$ and S1 values are higher than S2 values in the same range of q^2 for $I_{6s,\parallel}$. For $q^2 > 8$ GeV^2 the S1 and S2 values completely coincides for both $I_{5,\parallel}$ and $I_{6s,\parallel}$.

In $I_{5,\perp}$ and $I_{6s,\perp}$, values computed in SM and Z' S1 show maximum deviation from each other in the q^2 range from 0 to 6 GeV^2 where in case of $I_{5,\perp}$ S1 values are greater than SM and in case of $I_{6s,\perp}$ SM values are greater than S1 whereas from $q^2 > 6$ GeV^2 both values completely coincides for both cases. While comparing SM and Z' S2, values computed in both cases again coincides completely for all range of q^2 for both $I_{5,\perp}$ and $I_{6s,\perp}$. For the range of q^2= (0 to 10) GeV^2 Z' S1 values are greater than Z' S2 values for $I_{5,\perp}$ and Z' S2 values are greater than Z' S1 values for $I_{6s,\perp}$ whereas for q^2 >10 GeV^2 values in both Z' scenarios coincides again for both $I_{5,\perp}$ and $I_{6s,\perp}$. $I_{6c,\perp}$ is twice the $I_{6s,\perp}$.

$I_{6c,\parallel}$ is zero at all range of q^2. $I_{7,(\parallel,\perp)}$ has negligible values in SM and Z' S1 whereas it shows plot with small values in Z' S2. $I_{8,(\parallel,\perp)}$ and $I_{9,(\parallel,\perp)}$ has small values of order 10^3 GeV^2 in SM as well as in both scenarios of Z'.

Plots for Parallel Angular Coefficients

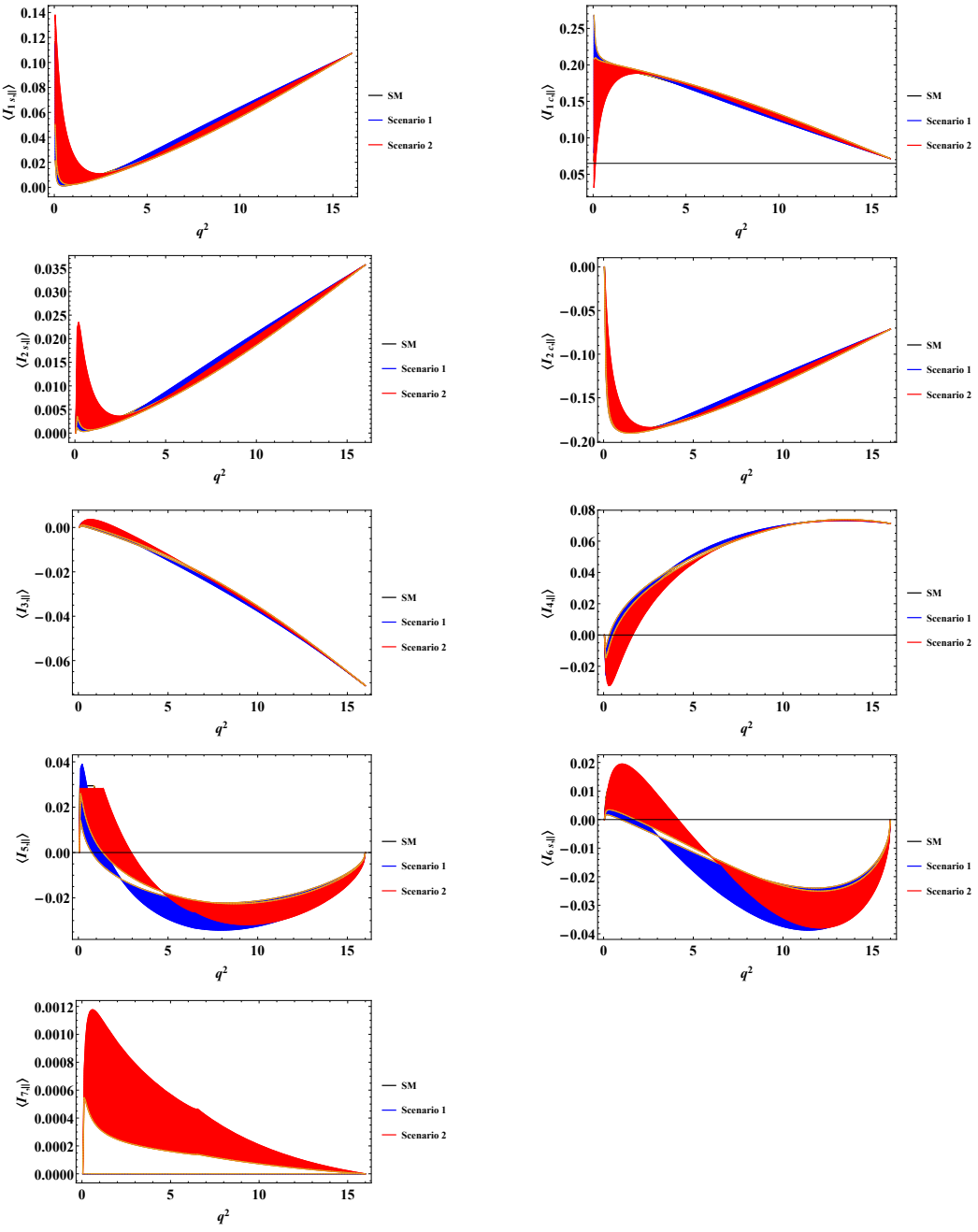

Figure 6.1: The angular coefficients $I_i(q^2)$ as a function of q^2 for longitudinally polarized ρ, plotted within SM along with family non universal Z' model for Scenario 1 and Scenario 2.The width of each curve is determined from the theoretical uncertainities associated with the $B \to a_1$ from factors.

Plots for Perpendicular Angular Coefficients

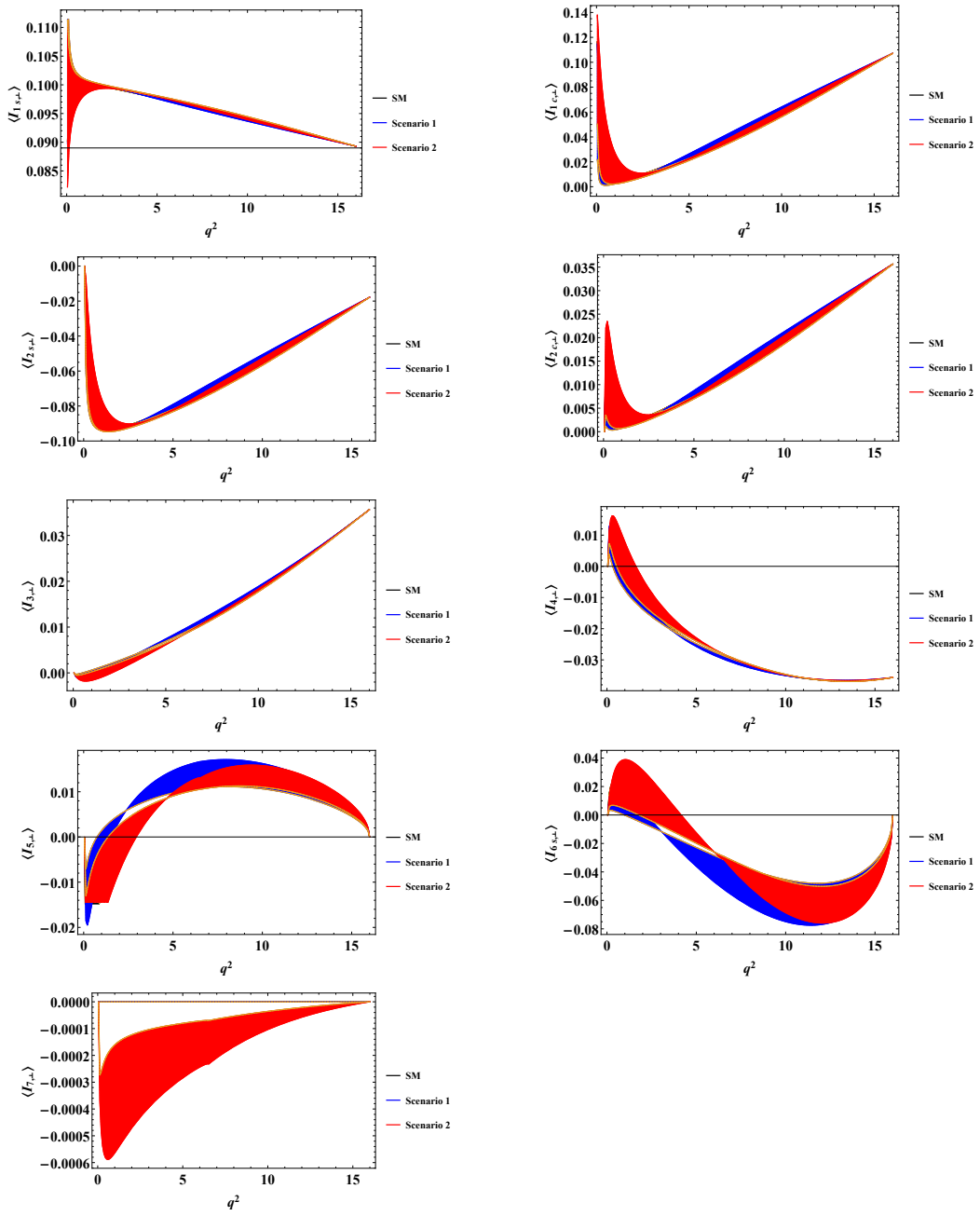

Figure 6.2: The angular coefficients $I_i(q^2)$ as a function of q^2 for transversely polarized ρ, plotted within SM along with family non universal Z' model for Scenario 1 and Scenario 2.The width of each curve is determined from the theoretical uncertainities associated with the $B \to a_1$ from factors.

6.2 Branching Ratio

The branching ratio refers to the proportion of instances in which a particle undergoes decay into a specific final state. It is the ratio of partial decay width to total decay width. In terms of differential decay distribution it is written as

$$\frac{d\Gamma}{dq^2} = \int_0^{2\pi} d\chi \int_0^{\pi} d(\sin\theta_V) \int_0^{\pi} d(\sin\theta) \frac{d^4\Gamma}{dq^2 d\theta d\theta_V d\chi} \tag{6.2.1}$$

For $B \to a_1(\to \rho\pi)l^+l^-$ decay in terms of angular coefficients it is computed as

$$\frac{d\Gamma}{dq^2} = \frac{1}{2}(\mathcal{N}_{\parallel}(I1c_{,\parallel} + 3I1s_{,\parallel} - I2s_{,\parallel}) + \mathcal{N}_{\perp}(I1c_{,\perp} + 3I1s_{,\perp} - I2s_{,\perp})) \tag{6.2.2}$$

Figure (6.1) shows plot of branching ratio for the values computed within SM and both scenarios of Z'. For all three cases the bands of BR are clearly distinguished. It can be seen that for small range of q^2 the band separation is greater whereas for large values of q^2 the bands become closer yet separated. The trend for all three cases is same for whole range of q^2. The values computed within SM lies in the centre with the Z' S1 values higher than SM and Z' S2 values lower than SM.

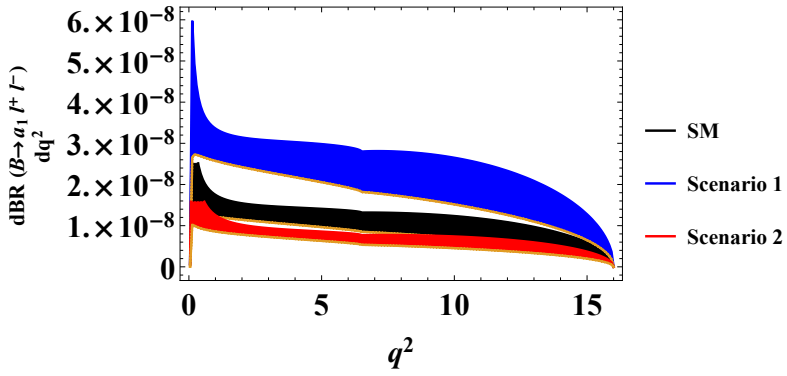

Figure 6.3: Branching Ratio for the decay $B \to a_1 l^+ l^-$ as a function of q^2, plotted within SM along with family non universal Z' model for Scenario 1 and Scenario 2. In the figure black band corresponds to SM, the blue and the red band corresponds to Scenario 1 and Scenario 2 of Z' model respectively. The width of each curve is determined from the theoretical uncertainities associated with the $B \to a_1$ from factors.

6.3 Forward Backward Asymmetry

FBA in terms of differential decay distribution is defined as

$$d\mathcal{FBA} = \int_0^{2\pi} d\chi \int_0^{\pi} d(\sin\theta_V) \int_0^{\frac{\pi}{2}} d(\sin\theta) \frac{d^4\Gamma}{dq^2 d\theta d\theta_V d\chi} - \int_0^{2\pi} d\chi \int_0^{\pi} d(\sin\theta_V) \int_{\frac{\pi}{2}}^{\pi} d(\sin\theta) \frac{d^4\Gamma}{dq^2 d\theta d\theta_V d\chi} \quad (6.3.1)$$

FBA for $B \to a_1(\to \rho\pi)l^+l^-$ in terms of angular coefficients is calculated as

$$d\mathcal{FBA} = \frac{3}{8}(\mathcal{N}_{\parallel}(I6c_{,\parallel} + 2I6s_{,\parallel}) + \mathcal{N}_{\perp}(I6c_{,\perp} + 2I6s_{,\perp})) \quad (6.3.2)$$

Normalized FBA is defined as

$$< d\mathcal{FBA} >= \frac{d\mathcal{FBA}}{\frac{d\Gamma}{dq^2}} \quad (6.3.3)$$

Normalized FBA for $B \to a_1(\to \rho\pi)l^+l^-$ decay in terms of angular coefficients is calculated as

$$< d\mathcal{FBA} >= \frac{3(\mathcal{N}_{\parallel}(I6c_{,\parallel} + 2I6s_{,\parallel}) + \mathcal{N}_{\perp}(I6c_{,\perp} + 2I6s_{,\perp}))}{4(\mathcal{N}_{\parallel}(I1c_{,\parallel} + 3I1s_{,\parallel} - I2s_{,\parallel}) + \mathcal{N}_{\perp}(I1c_{,\perp} + 3I1s_{,\perp} - I2s_{,\perp}))} \quad (6.3.4)$$

Figure (6.2) shows plot for the normalized FBA against q^2. For small range of q^2 the FBA computed within SM has highest values than both scenarios of Z'. This shows that the greatest asymmetry is present within SM. Next to SM the Z' S2 shows asymmetry and S1 has lowest values which means it exhibits the minimum asymmetry. For higher range of q^2 the values within SM and both Z' scenarios coincides and shows no notable difference in forward-backward asymmetry. Also these values are significantly deviated from 0 as can be seen in the figure below which clearly shows this deviation in the negative values of FBA.

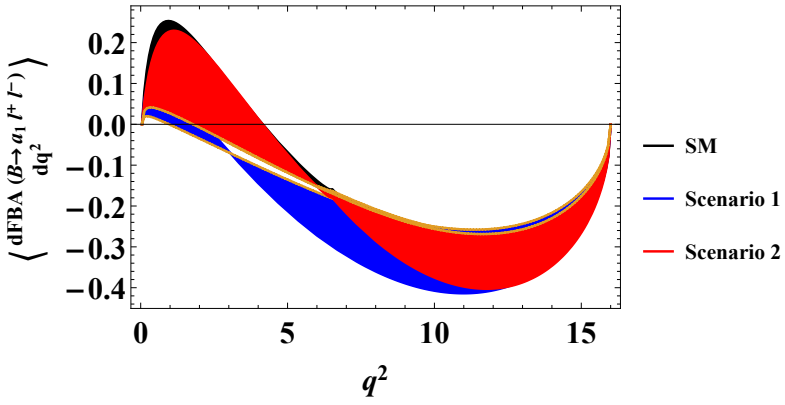

Figure 6.4: Normalized Forward Backward Asymmetry for the decay $B \to a_1 l^+ l^-$ as a function of q^2, plotted within SM along with family non universal Z' model for Scenario 1 and Scenario 2. In the figure black band corresponds to SM, the blue and the red band corresponds to Scenario 1 and Scenario 2 of Z' model respectively. The width of each curve is determined from the theoretical uncertainities associated with the $B \to a_1$ from factors.

Chapter 7

Conclusion

Investigating rare semileptonic decays of B mesons provides an avenue to explore physics that extends beyond the Standard Model. While there are numerous precise findings on processes induced by $b \to s l^+ l^-$ transitions, there is inadequate data available for $b \to d l^+ l^-$ induced decays. Within the literature, several exclusive semileptonic decays that involve FCNC transitions and FCCC transitions exhibit notable deviation from SM predictions.

Using effective Hamiltonian by putting the expressions of operators which resulted in matrix elements that includes Lorentz invariant vector, axial vector and tensor form factors, angular decay distribution is derived in terms of angular coefficients. Quantities of interest, like the branching ratio and forward-backward asymmetry, have been derived in terms of these angular coefficients. These physical observables along with angular coefficients are analyzed and plotted within SM and family non-universal Z' model.

Based on this research, findings have shown considerable deviations of New Physics scenarios from SM of the physical observables that are analyzed for the decay $B \to a_1 l^+ l^-$. Despite of large theoretical uncertainities in form factors for $B \to a_1$ decay, the estimates of NP outcomes remain consistent with those of the SM. For the branching ratio computed within SM and Z' S1 and S2, the S1 values have shown an increase whereas S2 values have shown decrease from SM values for all range of q^2. On the other hand values computed for Normalized FBA have shown deviations of Z' scenarios from SM for lower range of q^2 and for higher range values computed in all scenarios coincides and there is no notable difference observed. Angular coefficients computed within SM and Z' scenarios have shown very less deviation from SM values. These results clearly

indicate the need for more data to investigate NP through $B \to a_1$ channel.

In the time ahead, the measurement of these physical observables is anticipated to not only aid in the examination of Standard Model parameters but also facilitate the detection of Z' boson at the particle colliders.

Appendix

In this appendix, input parameters utilized in the calculations and the SM along with NP predictions of physical observables in different q^2 bins are given.

A: Numerical Input Parameters

m_B	m_{a1}	m_b	m_d	α_{em}^{-1}	G_F	V_{tb}	V_{td}
5.28 GeV	1.260 GeV	4.28 GeV	4.6 MeV	137	1.17 10 5 GeV^2	0.95	8.3×10^{-3}

Table 7.1: Input parameter values implemented in numerical analysis.

B: Binned Predictions of Physical Observables

Normalized FBA			
$q^2(GeV^2)$	**Standard Model**	Z' **Scenario 1**	Z' **Scenario 2**
[0.0 - 2.0]	$0.050^{+0.034}_{-0.040}$	$0.015^{+0.018}_{-0.014}$	$0.045^{+0.026}_{-0.036}$
[2.0 - 4.0]	$0.009^{+0.033}_{-0.027}$	$-0.028^{+0.002}_{-0.001}$	$0.009^{+0.034}_{-0.026}$
[4.0 - 6.0]	$-0.039^{+0.013}_{-0.008}$	$-0.071^{+0.013}_{-0.017}$	$-0.041^{+0.012}_{-0.006}$
[15.0 - 16.0]	$-0.068^{+0.010}_{-0.014}$	$-0.067^{+0.011}_{-0.016}$	$-0.070^{+0.011}_{-0.016}$

Table 7.2: Estimate of averaged values of normalized forward backward asymmetry , in different q^2 bins, for the SM as well as the Z' scenario 1 and scenario 2. The listed errors stem from uncertainties associated with the form factors.

$q^2 = 0.0 - 2.0\ GeV^2$			
Angular Observables	**Standard Model**	Z' **Scenario 1**	Z' **Scenario 2**
$I_{1s,\parallel}$	$0.088^{+0.094}_{-0.066}$	$0.037^{+0.043}_{-0.022}$	$0.109^{+0.118}_{-0.088}$
$I_{1c,\parallel}$	$0.896^{+0.130}_{-0.092}$	$0.975^{+0.061}_{-0.031}$	$0.873^{+0.166}_{-0.123}$
$I_{2s,\parallel}$	$0.024^{+0.025}_{-0.017}$	$0.010^{+0.011}_{-0.005}$	$0.029^{+0.032}_{-0.023}$
$I_{2c,\parallel}$	$-0.830^{+0.123}_{-0.085}$	$-0.872^{+0.055}_{-0.028}$	$-0.786^{+0.150}_{-0.110}$
$I_{3\parallel}$	$0.001^{+0.003}_{-0.005}$	$-0.001^{+0.003}_{-0.006}$	$0.007^{+0.005}_{-0.004}$
$I_{4\parallel}$	$0.008^{+0.020}_{-0.055}$	$0.024^{+0.011}_{-0.045}$	$-0.038^{+0.046}_{-0.003}$
$I_{5\parallel}$	$0.145^{+0.068}_{-0.111}$	$0.037^{+0.036}_{-0.029}$	$0.129^{+0.054}_{-0.098}$
$I_{6s,\parallel}$	$0.052^{+0.036}_{-0.042}$	$0.015^{+0.019}_{-0.014}$	$0.046^{+0.030}_{-0.037}$
$I_{6c,\parallel}$	0	0	0

Table 7.3: Estimate of averaged values of angular observables for longitudinally polarised ρ , in $q^2 = 0.0 - 2.0\ GeV^2$ bin, for the SM as well as the Z' scenario 1 and scenario 2. The listed errors stem from uncertainties associated with the form factors.

$q^2 = 2.0 - 4.0\ GeV^2$			
Angular Observables	**Standard Model**	Z' **Scenario 1**	Z' **Scenario 2**
$I_{1s,\parallel}$	$0.064^{+0.015}_{-0.007}$	$0.057^{+0.002}_{-0}$	$0.049^{+0.012}_{-0}$
$I_{1c,\parallel}$	$0.918^{+0.020}_{-0.010}$	$0.929^{+0.003}_{-0}$	$0.940^{+0.017}_{-0.001}$
$I_{2s,\parallel}$	$0.021^{+0.005}_{-0.002}$	$0.019^{+0.001}_{-0}$	$0.016^{+0.004}_{0}$
$I_{2c,\parallel}$	$-0.905^{+0.020}_{-0.010}$	$-0.908^{+0.003}_{-0}$	$-0.921^{+0.017}_{-0.001}$
$I_{3\parallel}$	$-0.032^{+0.001}_{-0.002}$	$-0.033^{+0.001}_{-0.002}$	$-0.023^{+0.005}_{-0.007}$
$I_{4\parallel}$	$0.167^{+0.009}_{-0.01}$	$0.174^{+0.005}_{-0.004}$	$0.140^{+0.024}_{-0.025}$
$I_{5\parallel}$	$-0.026^{+0.028}_{-0.029}$	$-0.078^{+0.007}_{-0.009}$	$-0.026^{+0.028}_{-0.027}$
$I_{6s,\parallel}$	$0.009^{+0.079}_{-0.003}$	$-0.029^{+0.002}_{-0.001}$	$0.009^{+0.035}_{-0.009}$
$I_{6c,\parallel}$	0	0	0

Table 7.4: Estimate of averaged values of angular observables for longitudinally polarised ρ , in $q^2 = 2.0 - 4.0\ GeV^2$ bin, for the SM as well as the Z' scenario 1 and scenario 2. The listed errors stem from uncertainties associated with the form factors.

$q^2 = 4.0 - 6.0\ GeV^2$			
Angular Observables	**Standard Model**	Z' **Scenario 1**	Z' **Scenario 2**
$I_{1s,\parallel}$	$0.123^{+0.014}_{-0.012}$	$0.121^{+0.008}_{-0.010}$	$0.105^{+0.006}_{-0.002}$
$I_{1c,\parallel}$	$0.838^{+0.019}_{-0.016}$	$0.842^{+0.012}_{-0.012}$	$0.863^{+0.009}_{-0.002}$
$I_{2s,\parallel}$	$0.041^{+0.005}_{-0.004}$	$0.040^{+0.003}_{-0.003}$	$0.035^{+0.002}_{-0.001}$
$I_{2c,\parallel}$	$-0.831^{+0.018}_{-0.016}$	$-0.831^{+0.012}_{-0.012}$	$-0.853^{+0.009}_{-0.002}$
$I_{3\parallel}$	$-0.070^{+0.002}_{-0.003}$	$-0.071^{+0.002}_{-0.003}$	$-0.061^{+0.001}_{-0.003}$
$I_{4\parallel}$	$0.245^{+0.001}_{-0.002}$	$0.248^{+0.003}_{-0.005}$	$0.229^{+0.005}_{-0.006}$
$I_{5\parallel}$	$-0.090^{+0.003}_{-0.001}$	$-0.122^{+0.021}_{-0.026}$	$-0.093^{+0.001}_{-0.005}$
$I_{6s,\parallel}$	$-0.041^{+0.013}_{-0.007}$	$-0.074^{+0.014}_{-0.018}$	$-0.043^{+0.013}_{-0.005}$
$I_{6c,\parallel}$	0	0	0

Table 7.5: Estimate of averaged values of angular observables for longitudinally polarised ρ , in $q^2 = 4.0 - 6.0\ GeV^2$ bin, for the SM as well as the Z' scenario 1 and scenario 2. The listed errors stem from uncertainties associated with the form factors.

$q^2 = 15.0 - 16.0\ GeV^2$			
Angular Observables	**Standard Model**	Z' **Scenario 1**	Z' **Scenario 2**
$I_{1s,\parallel}$	$0.480^{+0.001}_{-0.003}$	$0.480^{+0.001}_{-0.003}$	$0.479^{+0.002}_{-0.002}$
$I_{1c,\parallel}$	$0.360^{+0.002}_{-0.004}$	$0.361^{+0.003}_{-0.003}$	$^{0}.361+0.002_{-0.003}$
$I_{2s,\parallel}$	$0.160^{+0}_{-0.001}$	$0.159^{+0.001}_{-0}$	$0.159^{+0.001}_{-0}$
$I_{2c,\parallel}$	$-0.360^{+0.003}_{-0.003}$	$-0.359^{+0.002}_{-0.003}$	$-0.360^{+0.002}_{-0.001}$
$I_{3\parallel}$	-0.316^{+0}_{-0}	-0.316^{+0}_{-0}	-0.316^{+0}_{-0}
$I_{4\parallel}$	$0.338^{+0.001}_{-0.001}$	$0.337^{0}_{-0.001}$	$0.338^{+0.001}_{-0.001}$
$I_{5\parallel}$	$-0.043^{+0.005}_{-0.009}$	$-0.041^{+0.007}_{-0.009}$	$-0.043^{+0.007}_{-0.009}$
$I_{6s,\parallel}$	$-0.079^{+0.011}_{-0.016}$	$-0.077^{+0.013}_{-0.018}$	$-0.018^{+0.076}_{-0.045}$
$I_{6c,\parallel}$	0	0	0

Table 7.6: Estimate of averaged values of angular observables for longitudinally polarised ρ , in $q^2 = 15.0 - 16.0\ GeV^2$ bin, for the SM as well as the Z' scenario 1 and scenario 2. The listed errors stem from uncertainties associated with the form factors.

$q^2 = 0.0 - 2.0\ GeV^2$			
Angular Observables	**Standard Model**	Z' **Scenario 1**	Z' **Scenario 2**
$I_{1s,\perp}$	$0.492^{+0.018}_{-0.013}$	$0.506^{+0.009}_{-0.005}$	$0.491^{+0.024}_{-0.018}$
$I_{1c,\perp}$	$0.088^{+0.094}_{-0.066}$	$0.037^{+0.043}_{-0.022}$	$0.109^{+0.118}_{-0.088}$
$I_{2s,\perp}$	$-0.403^{+0.074}_{-0.051}$	$-0.431^{+0.033}_{-0.016}$	$-0.378^{+0.091}_{-0.067}$
$I_{2c,\perp}$	$0.024^{+0.025}_{-0.017}$	$0.010^{+0.011}_{-0.005}$	$0.029^{+0.032}_{-0.023}$
$I_{3\perp}$	$0.003^{+0.001}_{-0}$	$0.003^{+0}_{-0.001}$	$0.003^{+0}_{-0.001}$
$I_{4\perp}$	$-0.004^{+0.018}_{-0.027}$	$-0.012^{+0.018}_{-0.022}$	$0.019^{+0.023}_{-0.040}$
$I_{5\perp}$	$-0.072^{+0.035}_{-0.055}$	$-0.019^{+0.018}_{-0.023}$	$-0.065^{+0.027}_{-0.050}$
$I_{6s,\perp}$	$0.026^{+0.018}_{-0.021}$	$0.008^{+0.009}_{-0.009}$	$0.023^{+0.015}_{-0.018}$
$I_{6c,\perp}$	$0.052^{+0.036}_{-0.042}$	$0.015^{+0.019}_{-0.016}$	$0.046^{+0.030}_{-0.037}$

Table 7.7: Estimate of averaged values of angular observables for transversely polarised ρ , in $q^2 = 0.0 - 2.0\ GeV^2$ bin, for the SM as well as the Z' scenario 1 and scenario 2. The listed errors stem from uncertainties associated with the form factors.

$q^2 = 2.0 - 4.0\ GeV^2$			
Angular Observables	**Standard Model**	Z' **Scenario 1**	Z' **Scenario 2**
$I_{1s,\perp}$	$0.491^{+0.003}_{-0.001}$	0.493^{+0}_{-0}	$0.494^{+0.002}_{-0}$
$I_{1c,\perp}$	$0.064^{+0.015}_{-0.007}$	$0.057^{+0.002}_{-0}$	$0.049^{+0.012}_{-0}$
$I_{2s,\perp}$	$-0.442^{+0.013}_{-0.006}$	$-0.445^{+0.003}_{-0}$	$-0.452^{+0.010}_{-0}$
$I_{2c,\perp}$	$0.021^{+0.005}_{-0.002}$	$0.019^{+0.001}_{-0}$	-0.016$^{+0.004}_{-0}$
$I_{3\perp}$	$0.012^{+0.001}_{-0}$	0.012^{+0}_{-0}	$0.011^{+0}_{-0.001}$
$I_{4\perp}$	$-0.084^{+0.005}_{-0.004}$	$-0.087^{+0.002}_{-0.002}$	$-0.070^{+0.012}_{-0.013}$
$I_{5\perp}$	$-0.013^{+0.012}_{-0.040}$	$0.039^{+0.003}_{-0.005}$	$0.013^{+0.014}_{-0.014}$
$I_{6s,\perp}$	$0.005^{+0.016}_{-0.014}$	$-0.014^{+0.001}_{-0}$	$0.005^{+0.016}_{-0.003}$
$I_{6c,\perp}$	$0.009^{+0.034}_{-0.009}$	$-0.029^{+0.002}_{-0.001}$	$0.009^{+0.035}_{-0.009}$

Table 7.8: Estimate of averaged values of angular observables for transversely polarised ρ , in $q^2 = 2.0 - 4.0\ GeV^2$ bin, for the SM as well as the Z' scenario 1 and scenario 2. The listed errors stem from uncertainties associated with the form factors.

$q^2 = 4.0 - 6.0\ GeV^2$			
Angular Observables	**Standard Model**	Z' **Scenario 1**	Z' **Scenario 2**
$I_{1s,\perp}$	$0.480^{+0.002}_{-0.002}$	$0.481^{+0.001}_{-0.002}$	$0.484^{+0.001}_{-0}$
$I_{1c,\perp}$	$0.123^{+0.014}_{-0.012}$	$0.121^{+0.008}_{-0.010}$	$0.105^{+0.006}_{-0.002}$
$I_{2s,\perp}$	$-0.395^{+0.011}_{-0.010}$	$-0.396^{+0.008}_{-0.007}$	$-0.409^{+0.005}_{-0.001}$
$I_{2c,\perp}$	$0.041^{+0.005}_{-0.004}$	$0.040^{+0.003}_{-0.003}$	$0.035^{+0.002}_{-0.001}$
$I_{3\perp}$	$0.022^{+0.001}_{-0.001}$	$0.022^{+0.001}_{-0}$	$0.022^{+0.001}_{-0}$
$I_{4\perp}$	$-0.122^{+0.001}_{-0.001}$	$-0.124^{+0.002}_{-0.003}$	$-0.115^{+0.003}_{-0.003}$
$I_{5\perp}$	$0.045^{+0.001}_{-0.001}$	$0.061^{+0.010}_{-0.013}$	$0.046^{+0.001}_{-0.002}$
$I_{6s,\perp}$	$-0.021^{+0.007}_{-0.003}$	$-0.037^{+0.007}_{-0.009}$	$-0.021^{+0.006}_{-0.003}$
$I_{6c,\perp}$	$-0.041^{+0.013}_{-0.008}$	$-0.074^{+0.014}_{-0.018}$	$-0.043^{+0.013}_{-0.005}$

Table 7.9: Estimate of averaged values of angular observables for transversely polarised ρ , in $q^2 = 4.0 - 6.0\ GeV^2$ bin, for the SM as well as the Z' scenario 1 and scenario 2. The listed errors stem from uncertainties associated with the form factors.

$q^2 = 15.0 - 16.0\ GeV^2$			
Angular Observables	**Standard Model**	Z' **Scenario 1**	Z' **Scenario 2**
$I_{1s,\perp}$	0.420^{+0}_{-0}	$0.420^{+0}_{-0.001}$	$0.420^{+0}_{-0.001}$
$I_{1c,\perp}$	$0.480^{+0.001}_{-0.003}$	$0.480^{+0.001}_{-0.003}$	$0.479^{+0.002}_{-0.002}$
$I_{2s,\perp}$	$-0.100^{+0.001}_{-0.002}$	$-0.100^{+0.002}_{-0.002}$	$-0.100^{+0.001}_{-0.002}$
$I_{2c,\perp}$	$0.160^{+0}_{-0.001}$	$0.159^{+0.001}_{-0}$	$0.159^{+0.001}_{-0}$
$I_{3\perp}$	$0.139^{+0.003}_{-0.004}$	$0.138^{+0.003}_{-0.004}$	$0.139^{+0.003}_{-0.004}$
$I_{4\perp}$	-0.169^{+0}_{-0}	$-0.169^{+0.001}_{-0}$	-0.169^{+0}_{-0}
$I_{5\perp}$	$0.021^{+0.003}_{-0.004}$	$0.021^{+0.003}_{-0.005}$	$0.021^{+0.003}_{-0.005}$
$I_{6s,\perp}$	$-0.040^{+0.005}_{-0.008}$	$-0.039^{+0.006}_{-0.010}$	$-0.041^{+0.006}_{-0.010}$
$I_{6c,\perp}$	$-0.079^{+0.011}_{-0.016}$	$-0.078^{+0.012}_{-0.019}$	$-0.081^{+0.0130}_{-0.018}$

Table 7.10: Estimate of averaged values of angular observables for transversely polarised ρ , in $q^2 = 15.0 - 16.0\ GeV^2$ bin, for the SM as well as the Z' scenario 1 and scenario 2. The listed errors stem from uncertainties associated with the form factors.

References

[1] Paul Langacker. The standard model and beyond. *CRC Press*, 2010.

[2] Mark Thomson. Modern particle physics. *Cambridge University Press*, 2013.

[3] Dhiman Chakraborty. Introduction to high energy physics. *Lecture Notes*, 2010.

[4] Paolo Franzini. Elementary particle physics. *Lecture Notes*, 2009.

[5] Jure Zupan. Introduction to flavour physics. *arXiv:1903.05062 [hep-ph]*, 2(05062): 32, 2019.

[6] Y. Nir. Flavour physics and cp violation. *arXiv:1010.2666 [hep-ph]*, 1:34, 2010.

[7] Gino Isidori. Flavor physics and cp violation. *arXiv:1302.0661v1 [hep-ph]*, 1, 2013.

[8] Nicola Cabibbo. Unitary symmetry and leptonic decays. *Phys. Rev. Lett.*, 10(12), 1963.

[9] M. Kobayashi and T. Maskawa. Cp violation in the renormalizable theory of weak interaction. *Phys. Rev. Lett.*, 49(2):6, 1973.

[10] C. Amsler et al. (Particle Data Group). The review of particle physics. *Phys. Lett. B667*, 1, 2008.

[11] Yuval Grossman. Introduction to flavor physics. *arXiv:1006.3534v1 [hep-ph]*, 1:45, 2010.

[12] C. Jarlskog. Commutator of the quark mass matrices in the standard electroweak model and a measure of maximal cp nonconservation. *Phys. Rev. Lett.*, 55(10), 1985.

[13] Luciano Maiani. The gim mechanism: origin, predictions and recent uses. *arXiv:1303.6154v1 [hep-ph]*, 1, 2013.

[14] Yosef Nir. The standard model and flavor physics. 2017.

[15] Matthias Neubert. Effective field theory and heavy quark physics. *arXiv:0512222 [hep-ph]*, 1:39, 2005.

[16] Andrzej J. Buras and Robert Fleischer. Quark mixing, cp violation and rare decays after the top quark discovery. *arXiv:9704376 [hep-ph]*, 1:180, 1997.

[17] Andrzej J. Buras Gerhard Buchalla and Markus E. Lautenbacher. Weak decays beyond leading logarithms. *Rev. Mod. Phys*, 68:1125–1244, 1996.

[18] Andrzej J. Buras. Operator product expansion, renormalization group and weak decays. *arXiv:9901409 [hep-ph]*, 1:24, 1999.

[19] M Ali Paracha. Investigating family non universal z' model via semileptonic $b \to a_1 l^+ l^-$ decays. *Physica Scripta*, 95(105304):12, 2020.

[20] R. Khosravi S. Momeni and F. Falahati. Flavor changing neutral current transition of b to a1 with light-cone sum rules. *Phys. Rev.*, 95(016009), 2017.

[21] P Nayek and S Sahoo. Study of semileptonic decay $b \to \rho l^+ l^-$in non-universal z' model. *Indian Journal of Pure Applied Physics*, 57:652–654, 2019.

[22] Paul Langacker. The physics of heavy z' gauge bosons. *arXiv:0801.1345v3 [hep-ph]*, 3, 2009.